

Title	Plankton networks driving carbon export in the oligotrophic ocean.
Author(s)	Guidi, Lionel; Chaffron, Samuel; Bittner, Lucie; Eveillard, Damien; Larhlimi, Abdelhalim; Roux, Simon; Darzi, Yousef; Audic, Stephane; Berline, Léo; Brum, Jennifer R; Coelho, Luis Pedro; Espinoza, Julio Cesar Ignacio; Malviya, Shruti; Sunagawa, Shinichi; Dimier, Céline; Kandels-Lewis, Stefanie; Picheral, Marc; Poulain, Julie; Searson, Sarah; Tara Oceans Consortium Coordinators; Stemmann, Lars; Not, Fabrice; Hingamp, Pascal; Speich, Sabrina; Follows, Mick; Karp-Boss, Lee; Boss, Emmanuel; Ogata, Hiroyuki; Pesant, Stephane; Weissenbach, Jean; Wincker, Patrick; Acinas, Silvia G; Bork, Peer; de Vargas, Colomban; Iudicone, Daniele; Sullivan, Matthew B; Raes, Jeroen; Karsenti, Eric; Bowler, Chris; Gorsky, Gabriel
Citation	Nature (2016), 532(7600): 465-470
Issue Date	2016-04-28
URL	<a href="http://hdl.handle.net/2433/210237">http://hdl.handle.net/2433/210237</a>
Right	This is the accepted version of the article, which has been published in final form at <a href="http://dx.doi.org/10.1038/nature16942">http://dx.doi.org/10.1038/nature16942</a> ; The full-text file will be made open to the public on 28 October 2016 in accordance with publisher's 'Terms and Conditions for Self-Archiving'.; This is not the published version. Please cite only the published version. この論文は出版社版ではありません。引用の際には出版社版をご確認ご利用ください。
Type	Journal Article
Textversion	author

1 **Title:**

2 **Plankton networks driving carbon export in the oligotrophic ocean**

3  
4 **Authors:** Lionel Guidi<sup>1,2,\*</sup>, Samuel Chaffron<sup>3,4,5,\*</sup>, Lucie Bittner<sup>6,7,8,\*</sup>, Damien Eveillard<sup>9,\*</sup>,  
5 Abdelhalim Larhlimi<sup>9</sup>, Simon Roux<sup>10,11</sup>, Youssef Darzi<sup>3,4</sup>, Stephane Audic<sup>8</sup>, Léo Berline<sup>1,12</sup>,  
6 Jennifer Brum<sup>10,11</sup>, Luis Pedro Coelho<sup>13</sup>, Julio Cesar Ignacio Espinoza<sup>10</sup>, Shruti Malviya<sup>7</sup>,  
7 Shinichi Sunagawa<sup>13</sup>, Céline Dimier<sup>8</sup>, Stefanie Kandels-Lewis<sup>13,14</sup>, Marc Picheral<sup>1</sup>, Julie  
8 Poulain<sup>15</sup>, Sarah Searson<sup>1,2</sup>, Tara Oceans coordinators, Lars Stemmann<sup>1</sup>, Fabrice Not<sup>8</sup>,  
9 Pascal Hingamp<sup>16</sup>, Sabrina Speich<sup>17</sup>, Mick Follows<sup>18</sup>, Lee Karp-Boss<sup>19</sup>, Emmanuel Boss<sup>19</sup>,  
10 Hiroyuki Ogata<sup>20</sup>, Stephane Pesant<sup>21,22</sup>, Jean Weissenbach<sup>15,23,24</sup>, Patrick Wincker<sup>15,23,24</sup>,  
11 Silvia G. Acinas<sup>25</sup>, Peer Bork<sup>13,26</sup>, Colomban de Vargas<sup>8</sup>, Daniele Iudicone<sup>27</sup>, Matthew B.  
12 Sullivan<sup>10,11</sup>, Jeroen Raes<sup>3,4,5</sup>, Eric Karsenti<sup>7,14</sup>, Chris Bowler<sup>7</sup>, Gabriel Gorsky<sup>1</sup>

13 \* These authors contributed equally to this work

14 **Affiliations:**

- 15 <sup>1</sup> Sorbonne Universités, UPMC Université Paris 06, CNRS, Laboratoire d’océanographie de Villefranche (LOV),  
16 Observatoire Océanologique, Villefranche-sur-Mer, France  
17 <sup>2</sup> Department of Oceanography, University of Hawaii, Honolulu, Hawaii, USA  
18 <sup>3</sup> Department of Microbiology and Immunology, Rega Institute, KU Leuven, Herestraat 49, 3000 Leuven, Belgium.  
19 <sup>4</sup> Center for the Biology of Disease, VIB, Herestraat 49, 3000 Leuven, Belgium.  
20 <sup>5</sup> Department of Applied Biological Sciences, Vrije Universiteit Brussel, Pleinlaan 2, 1050 Brussels, Belgium.  
21 <sup>6</sup> Sorbonne Universités, UPMC Univ Paris 06, CNRS, Institut de Biologie Paris-Seine (IBPS), Evolution Paris Seine, F-  
22 75005, Paris, France.  
23 <sup>7</sup> Ecole Normale Supérieure, PSL Research University, Institut de Biologie de l’Ecole Normale Supérieure (IBENS), CNRS  
24 UMR 8197, INSERM U1024, 46 rue d’Ulm, F-75005 Paris, France.  
25 <sup>8</sup> Sorbonne Universités, UPMC Université Paris 06, CNRS, Laboratoire Adaptation et Diversité en Milieu Marin, Station  
26 Biologique de Roscoff, Roscoff, France  
27 <sup>9</sup> LINA UMR 6241, Université de Nantes, EMN, CNRS, 44322 Nantes, France.  
28 <sup>10</sup> Department of Ecology and Evolutionary Biology, University of Arizona, Tucson, AZ, 85721, USA.  
29 <sup>11</sup> Current affiliation: Department of Microbiology, The Ohio State University, Columbus OH 43210, USA  
30 <sup>12</sup> Current affiliation: Aix-Marseille Univ., Mediterranean Institute of Oceanography (MIO), 13288, Marseille, Cedex 09,  
31 France ; Université du Sud Toulon-Var, MIO, 83957, La Garde cedex, France ; CNRS/INSU, MIO UMR 7294; IRD,  
32 MIO UMR235.  
33 <sup>13</sup> Structural and Computational Biology, European Molecular Biology Laboratory, Meyerhofstr. 1, 69117 Heidelberg,  
34 Germany,  
35 <sup>14</sup> Directors’ Research European Molecular Biology Laboratory Meyerhofstr. 1 69117 Heidelberg Germany,  
36 <sup>15</sup> CEA - Institut de Génomique, GENOSCOPE, 2 rue Gaston Crémieux, 91057 Evry France.  
37 <sup>16</sup> Aix Marseille Université CNRS IGS UMR 7256 13288 Marseille France  
38 <sup>17</sup> Department of Geosciences, Laboratoire de Météorologie Dynamique (LMD), Ecole Normale Supérieure, 24 rue  
39 Lhomond 75231 Paris Cedex 05 France.  
40 <sup>18</sup> Dept of Earth, Atmospheric and Planetary Sciences, Massachusetts Institute of Technology, Cambridge, USA.  
41 <sup>19</sup> School of Marine Sciences, University of Maine, Orono, USA.  
42 <sup>20</sup> Institute for Chemical Research, Kyoto University, Gokasho, Uji, Kyoto, 611-0011, Japan.  
43 <sup>21</sup> PANGAEA, Data Publisher for Earth and Environmental Science, University of Bremen, Bremen, Germany.  
44 <sup>22</sup> MARUM, Center for Marine Environmental Sciences, University of Bremen, Bremen, Germany.  
45 <sup>23</sup> CNRS, UMR 8030, CP5706, Evry France.  
46 <sup>24</sup> Université d’Evry, UMR 8030, CP5706, Evry France.  
47 <sup>25</sup> Department of Marine Biology and Oceanography, Institute of Marine Sciences (ICM)-CSIC Pg. Marítim de la  
48 Barceloneta 37-49 Barcelona E08003 Spain.  
49 <sup>26</sup> Max-Delbrück-Centre for Molecular Medicine, 13092 Berlin, Germany,  
50 <sup>27</sup> Stazione Zoologica Anton Dohrn, Villa Comunale, 80121, Naples, Italy.

51 **The biological carbon pump is the process by which CO<sub>2</sub> is transformed to organic**  
52 **carbon *via* photosynthesis, exported through sinking particles, and finally sequestered**  
53 **in the deep ocean or sediment. While the intensity of the pump correlates with plankton**  
54 **community composition, the underlying ecosystem structure and interactions driving**  
55 **the process remain largely uncharacterised. Here we use environmental and**  
56 **metagenomic data gathered during the *Tara* Oceans expedition to improve our**  
57 **understanding of carbon export in the oligotrophic ocean. We show that specific**  
58 **euphotic plankton communities correlate with carbon export and highlight unexpected**  
59 **and overlooked taxa such as Radiolaria, alveolate parasites, as well as *Synechococcus***  
60 **and their phages, as lineages most strongly associated with carbon export in the**  
61 **subtropical, nutrient-depleted, oligotrophic ocean. Additionally, we show that the**  
62 **relative abundance of just a few bacterial and viral genes can predict most of the**  
63 **variability in carbon export in these regions.**

64 Marine planktonic photosynthetic organisms are responsible for approximately fifty percent  
65 of Earth's primary production and they fuel the global ocean biological carbon pump<sup>1</sup>. The  
66 intensity of the pump is correlated to plankton community composition<sup>2,3</sup>, and controlled by  
67 the relative rates of primary production and carbon remineralisation<sup>4</sup>. About 10% of this  
68 newly produced organic carbon in the surface ocean is exported through gravitational  
69 sinking of particles. Finally, after multiple transformations, only a fraction of the exported  
70 material will reach the deep ocean where it is sequestered over thousand-year timescales of  
71 the ocean's overturning circulation<sup>5</sup>.

72 Like most biological systems, marine ecosystems in the sunlit upper layer of the ocean  
73 (denoted the euphotic zone) are complex<sup>6,7</sup>, characterised by a wide range of biotic and  
74 abiotic interactions<sup>8-10</sup> and in constant balance between carbon production, transfer to higher

75 trophic levels, remineralisation, and export to the deep layers<sup>11</sup>. The marine ecosystem  
76 structure and its taxonomic and functional composition likely evolved to comply with this  
77 loss of energy by modifying organism turnover times and by the establishment of complex  
78 feedbacks between them<sup>6</sup> and the substrates they can exploit for metabolism<sup>12</sup>. Decades of  
79 groundbreaking research have focused on identifying independently the key players involved  
80 in the biological carbon pump. Among autotrophs, diatoms are commonly attributed to being  
81 important in carbon flux because of their large size and fast sinking rates<sup>13-15</sup> while small  
82 autotrophic picoplankton may contribute directly as a result of subduction of surface water  
83 resulting from sub-mesoscale dynamic features<sup>16</sup> or indirectly by aggregating with larger  
84 settling particles or through their consumption by organisms at higher trophic levels<sup>17</sup>.  
85 Among heterotrophs, zooplankton such as copepods impact carbon flux *via* production of  
86 fast-sinking fecal pellets while migrating hundreds of meters in the water-column<sup>18,19</sup>. These  
87 observations, focusing on just a few components of the marine ecosystem, highlight that  
88 carbon export results from multiple biotic interactions and that a better understanding of the  
89 mechanisms involved in its regulation will likely require an analysis of the entire planktonic  
90 ecosystem.

91 Advanced sequencing technologies now offer the opportunity to simultaneously survey  
92 whole planktonic communities and associated molecular functions in unprecedented detail.  
93 Such a holistic approach may allow the identification of community- or gene-based  
94 biomarkers that could be used to monitor and predict ecosystem functions, e.g., related to the  
95 biogeochemistry of the ocean<sup>20-22</sup>. Here, we leverage global-scale ocean genomics  
96 datasets<sup>10,23-25</sup> and associated environmental data to assess the coupling between ecosystem  
97 structure, functional repertoire, and the carbon export component of the biological carbon  
98 pump.

## 99 **Carbon export and plankton community composition**

100 The *Tara* Oceans global circumnavigation crossed diverse ocean ecosystems and sampled  
101 plankton at an unprecedented scale<sup>20,26</sup> (see Methods). Hydrographic data were measured *in*  
102 *situ* or in seawater samples at all stations, as well as nutrients, oxygen and photosynthetic  
103 pigments (see Methods). Net Primary Production (NPP) was derived from satellite  
104 measurements (see Methods). In addition, particle size distributions (100  $\mu\text{m}$  to a few mm)  
105 and concentrations were measured using an Underwater Vision Profiler (UVP) from which  
106 carbon export, corresponding to the carbon flux (Fig. 1) at 150 m, was calculated to range  
107 from 0.014 to 18.3  $\text{mg}\cdot\text{m}^{-2}\cdot\text{d}^{-1}$  using previously validated methods (see Methods). The  
108 approach allowed us to assemble the largest homogeneous carbon flux dataset during a  
109 single expedition, corresponding to more than 600 profiles over 150 stations. This dataset is  
110 of similar magnitude to the body of historical data available in the literature that includes the  
111 134 deep sediment trap-based carbon flux time-series<sup>27</sup> from the JGOFS program and the  
112 419 thorium-derived particulate organic carbon (POC) export measurements<sup>28</sup>.

113 From 68 globally distributed sites, a total of 7.2 Tb of metagenomics data, representing *circa*  
114 40 million non-redundant genes, around 35,000 Operational Taxonomic Units (OTUs) of  
115 prokaryotes (Bacteria and Archaea) and numerous mainly uncharacterized viruses and  
116 picoeukaryotes, have been described recently<sup>23,25</sup>. In addition, a set of 2.3 million eukaryotic  
117 18S rDNA ribotypes was generated from a subset of 47 sampling sites corresponding to  
118 approximately 130,000 OTUs<sup>24</sup>. Finally, 5,476 viral “populations” were identified at 43 sites  
119 from viral metagenomic contigs, only 39 (<0.1%) of which had been previously observed<sup>25</sup>  
120 (see Methods). These genomics data combined across all domains of life together with  
121 carbon flux estimates and other environmental parameters were used to explore the  
122 relationships between marine biogeochemistry and euphotic plankton communities (see

123 Methods) in the oligotrophic open ocean. Our study did not include high latitude areas due to  
124 the current lack of available molecular data.

125 Using a method for regression-based modeling of high dimensional data in biology  
126 (specifically a sparse Partial Least Square analysis - sPLS<sup>29</sup>, Extended data Fig. 1), we  
127 detected several plankton lineages for which relative sequence abundance correlated with  
128 carbon export and other environmental parameters, most notably with NPP, as expected (Fig.  
129 2 and see Supplementary Information SII). These included diatoms, dinoflagellates and  
130 metazoa (zooplankton), lineages classically identified as key contributors to carbon export.

### 131 **Plankton community networks associated with carbon export**

132 While the analysis presented in Fig. 2 supports previous findings about key organisms  
133 involved in carbon export from the euphotic zone<sup>14,15,17-19</sup>, it is not able to capture how the  
134 intrinsic structure of the planktonic community relates to this biogeochemical process.  
135 Conversely, although other recent holistic approaches<sup>10,30,31</sup> used species co-occurrence  
136 networks to reveal potential biotic interactions, they do not provide a robust description of  
137 sub-communities driven by abiotic interactions. To overcome these issues, we applied a  
138 systems biology approach known as Weighted Gene Correlation Network Analysis  
139 (WGCNA<sup>32,33</sup>) to detect significant associations between the *Tara* Oceans genomics data and  
140 carbon export. This method delineates communities in the euphotic zone that are the most  
141 associated with carbon export rather than predicting organisms associated with sinking  
142 particles.

143 In brief, the WGCNA approach builds a network in which nodes are features (in this case  
144 plankton lineages or gene functions) and links are evaluated by the robustness of co-  
145 occurrence scores. WGCNA then clusters the network into modules (hereafter denoted  
146 subnetworks) that can be examined to find strong and significant subnetwork-trait

147 relationships. We then filtered each subnetwork using a Partial Least Square (PLS) analysis  
148 that emphasizes key nodes (based on the Variable Importance in Projection (VIP) scores; see  
149 Methods and Extended data Fig. 1). These particular nodes are mandatory to summarize a  
150 subnetwork (or community) related to carbon export. In particular, they are of interest for  
151 evaluating (i) subnetwork robustness and (ii) predictive power for a given trait (see Methods  
152 and Extended data Fig. 1).

153 We applied WGCNA to the relative abundance tables of eukaryotic, prokaryotic and viral  
154 lineages<sup>23-25</sup> and identified unique subnetworks significantly associated with carbon export  
155 within each dataset (see Methods and Supplementary Information SI1, SI2, SI3). The  
156 eukaryotic subnetwork (subnetwork-trait relationship to carbon export, Pearson cor. = 0.81,  $p$   
157 =  $5e^{-15}$ ) contained 49 lineages (Extended data Fig. 2a and Supplementary Information SI2)  
158 among which twenty percent represented photosynthetic organisms (Fig. 3a and  
159 Supplementary Information SI2). Surprisingly, this small subnetwork's structure correlates  
160 very strongly to carbon export (Pearson cor. = 0.87,  $p = 5e^{-16}$ , Extended data Fig. 2d) and it  
161 predicts as much as 69% (Leave-One-Out Cross-Validated (LOOCV),  $R^2 = 0.69$ ) of the  
162 variability in carbon export (Extended data Fig. 3a). Only ~6% of the subnetwork nodes  
163 correspond to diatoms and they show lower VIP scores than dinoflagellates (Supplementary  
164 Information SI2). This is likely because our samples are not from silicate replete conditions  
165 where diatoms were blooming (see Methods). Furthermore, our analysis did not incorporate  
166 data from high latitudes, where diatoms are known to be particularly important for carbon  
167 export, so this result suggests that dinoflagellates have a heretofore unrecognized role in  
168 carbon export processes in subtropical oligotrophic 'type' ecosystems, one of the largest  
169 biome on Earth. More precisely four of the five highest VIP scoring eukaryotic lineages that  
170 correlated with carbon flux were heterotrophs such as Metazoa (copepods), non-  
171 photosynthetic Dinophyceae, and Rhizaria (Fig. 3a and Supplementary Information SI2).

172 These results corroborate recent metagenomics analysis of microbial communities from  
173 sediment traps in the oligotrophic North Pacific subtropical gyre<sup>34</sup>. Consistently, *in situ*  
174 imaging surveys have revealed Rhizarian lineages, made up of large fragile organisms such  
175 as the Collodaria, to represent an until now under-appreciated component of global plankton  
176 biomass<sup>35</sup>, which here also appear to be of relevance for carbon export. Another 14% of  
177 lineages from the subnetwork correspond to parasitic organisms, a largely under-explored  
178 component of planktonic ecosystems.

179 The prokaryotic subnetwork that associated most significantly with carbon export  
180 (subnetwork-trait relationship to carbon export, Pearson cor. = 0.32,  $p = 9e^{-03}$ ) contained 109  
181 OTUs (Extended data Fig. 2b and Supplementary Information SI3), its structure correlated  
182 well to carbon export (Pearson cor. = 0.47,  $p = 5e^{-06}$ , Extended data Fig. 2e) and it could  
183 predict as much as 60% of the carbon export (LOOCV,  $R^2 = 0.60$ ) (Extended data Fig. 3b).  
184 By far the highest VIP score within this community was assigned to *Synechococcus*,  
185 followed by *Cobetia*, *Pseudoalteromonas* and *Idiomarina*, as well as *Vibrio* and *Arcobacter*  
186 (Fig. 3b and Supplementary Information SI3). Noteworthy, *Prochlorococcus* genera and  
187 SAR11 clade fall out of this community, while the significance of *Synechococcus* for carbon  
188 export could be validated using absolute cell counts estimated by flow cytometry (Pearson  
189 cor. = 0.64,  $p = 4e^{-10}$ , Extended data Fig. 4b). Moreover, *Prochlorococcus* cell counts did not  
190 correlate with carbon export (Pearson cor. = -0.13,  $p = 0.27$ , Extended data Fig. 4a) whereas  
191 the *Synechococcus* to *Prochlorococcus* cell count ratio correlated positively and significantly  
192 (Pearson cor. = 0.54,  $p = 4e^{-07}$ , Extended data Fig. 4c), suggesting the relevance of  
193 *Synechococcus*, rather than *Prochlorococcus*, to carbon export. Interestingly,  
194 *Pseudoalteromonas*, *Idiomarina*, *Vibrio* and *Arcobacter* (of which several species are known  
195 to be associated with eukaryotes<sup>36</sup>) have also been observed in live and poisoned sediment  
196 traps<sup>34</sup> and these genera display very high VIP scores in our subnetwork associated with



197 carbon export. Additional genera reported as being enriched in poisoned traps (also known  
198 as being associated with eukaryotes) include *Enterovibrio* and *Campylobacter*, and are  
199 present as well in our carbon export subnetwork.

200 Interestingly, the viral subnetwork ( $n=277$ ) most related to carbon export (Pearson cor. =  
201 0.93,  $p = 2e^{-15}$ , Extended data Fig. 2c) contained particularly high VIP scores for two  
202 *Synechococcus* phages (Fig. 3c and Supplementary Information SI4), which represented a  
203 16-fold enrichment (Fisher's exact test  $p = 6.4e^{-09}$ ). Its structure also correlated with carbon  
204 export (Pearson cor. = 0.88,  $p = 6e^{-93}$ , Extended data Fig. 2f) and it could predict up to 89%  
205 of the variability of carbon export (LOOCV,  $R^2 = 0.89$ ) (Extended data Fig. 3c). The  
206 significance of these convergent results is reinforced by the fact that sequences from these  
207 datasets are derived from organisms collected on independent size filters (see Methods), and  
208 further implicates the importance of top-down processes in carbon export.

209 With the aim of integrating eukaryotic, prokaryotic, and viral carbon export communities, we  
210 synthesized their respective subnetworks using, as a backbone, a single global co-occurrence  
211 network established previously<sup>10</sup>. The resulting network focused on key lineages and their  
212 predicted co-occurrences (Fig. 4). Lineages with high VIP values (such as *Synechococcus*)  
213 are revealed here as hubs of the co-occurrence network<sup>10</sup>, illustrating the potentially strategic  
214 key roles within the integrated network of lineages under-appreciated by conventional  
215 methods to study carbon export in the ocean. Associations between the hub lineages are  
216 mostly mutually exclusive which may explain the relatively weak correlation of some of  
217 these lineages with carbon export when using standard correlation analyses as shown in Fig.  
218 2.

## 219 **Gene functions associated with carbon export**

220 Given the potential importance of prokaryotic processes influencing the biological carbon

221 pump<sup>22</sup>, we used the same analytical approaches to examine the prokaryotic genomic  
222 functions associated with carbon export in the annotated Ocean Microbial Reference Gene  
223 Catalogue from *Tara* Oceans<sup>23</sup>. We built a global co-occurrence network for functions (i.e.,  
224 Orthologous Groups of genes or OGs) from the euphotic zone and identified two  
225 subnetworks of functions that are significantly associated with carbon export (Fig. 5a,  
226 Extended data Fig. 5a, light and dark green subnetworks; FNET1 and FNET2, respectively,  
227 and Extended data Fig. 5c).

228 The majority of functions in FNET1 and FNET2 correlate well with carbon export (FNET1:  
229 mean Pearson cor. = 0.45, s.d. 0.09 and FNET2: mean Pearson cor. = 0.34, s.d. 0.10).  
230 Interestingly, FNET2 functions ( $n=220$ ) encode mostly (83%) core functions (i.e., functions  
231 observed in all euphotic samples, see Methods) while the majority of FNET1 functions  
232 ( $n=441$ ) are non-core (85%) (see Supplementary Information SI5, SI6), highlighting both  
233 essential and adaptive ecological functions associated with carbon export. Top VIP scoring  
234 functions in the FNET1 subnetwork are membrane proteins such as ABC-type sugar  
235 transporters (Fig. 5a). This subnetwork also contains many functions specific to the  
236 *Synechococcus* accessory photosynthetic apparatus (e.g., relating to phycobilisomes,  
237 phycocyanin and phycoerythrin; see Supplementary Information SI5), which is consistent  
238 with the major role of this genus for carbon export inferred from the prokaryotic subnetwork  
239 (Fig. 3b). In addition, functions related to carbohydrates, inorganic ion transport and  
240 metabolism, as well as transcription, are also well represented (Fig. 5b), suggesting overall a  
241 subnetwork of functions dedicated to photosynthesis and growth.

242 The FNET2 subnetwork contains several functions encoded by genes taxonomically  
243 assigned to *Candidatus pelagibacter* and *Prochlorococcus*, known as occupying similar  
244 oceanic regions as *Synechococcus*, but overall most of its relative abundance (74%) is

245 taxonomically unclassified (Extended data Fig. 6). Top VIP scoring functions in FNET2 are  
246 also membrane proteins and ABC-type sugar transporters, as well as functions involved in  
247 carbohydrate breakdown such as a chitinase (Fig. 5a). These features highlight the potential  
248 roles of bacteria in the formation and degradation of marine aggregates<sup>37</sup>. Strikingly, 77%  
249 and 58%, of OGs with a VIP score > 1 in FNET1 and FNET2, respectively, are functionally  
250 uncharacterized<sup>38,39</sup> (Fig. 5b), pointing to the strong need for future molecular work to  
251 explore these functions (see Supplementary Information SI5, SI6).

252 The relevance of the identified bacterial functions to predict carbon export was also  
253 confirmed by PLS regression (Extended data Fig. 6b and 6c). As proposed for plankton  
254 communities, the functional subnetworks predict 41% and 48% of carbon export variability  
255 (LOOCV,  $R^2 = 0.41$  and  $0.48$  for FNET1 and FNET2, respectively) with a minimal number  
256 of functions (Fig. 5b, 123 and 54 functions with a VIP score > 1 for FNET1 and FNET2,  
257 respectively). Finally, higher predictive power was obtained using subnetworks of viral  
258 protein clusters (Extended data Fig. 5b, 5d and 7a), predicting 55% and 89% of carbon  
259 export variability (LOOCV  $R^2 = 0.55$  and  $0.89$  for VNET1 and VNET2, respectively;  
260 Extended data Fig. 7b, Supplementary Information, SI7, SI8), suggesting again the key role,  
261 of not only bacteria, but also their phages in biological processes sustaining carbon export at  
262 a global level.

## 263 **Discussion**

264 In this report we have revealed the potential contribution of under-appreciated components  
265 of plankton communities, as well as confirmed the importance of prokaryotes and viruses, in  
266 the carbon export component of the biological carbon pump in the nutrient-depleted  
267 oligotrophic ocean. Carbon export was estimated from particle size distribution at 150 m  
268 measured with the UVP, and we assumed similar particle composition across all size classes.

269 Furthermore, because of instrument and method limitations, particles smaller than 250  $\mu\text{m}$   
270 were not used for these estimations (see Methods). These export estimates evaluate how  
271 much carbon leaves the euphotic zone, but they are not necessarily related to sequestration,  
272 which occurs deeper in the water column and over longer timescales. Overall, the use of the  
273 UVP was the only realistic method to evaluate carbon flux over the 3 years expedition  
274 because deployment of sediment traps at all stations would have been impossible. While our  
275 findings are consistent with the numerous previous studies that have highlighted the central  
276 role of copepods and diatoms in the biological carbon pump<sup>14,15,17-19</sup>, they place them in an  
277 ecosystem context and generate hypotheses as to the processes that determine the intensity of  
278 export, such as parasitism and predation. For example, while viruses are commonly assumed  
279 to lyse cells and maintain fixed organic carbon in surface waters, thereby reducing the  
280 intensity of the biological carbon pump<sup>40</sup>, there are hints that viral lysis may increase carbon  
281 export through the production of colloidal particles and aggregate formation<sup>41</sup>. Our current  
282 study suggests that these latter roles may be more ubiquitous than currently appreciated. The  
283 importance of aggregation and cell stickiness as inferred from gene network analysis, should  
284 be further explored mechanistically to investigate the biological significance of these  
285 findings.

286 The future evolution of the oceanic carbon sink remains uncertain because of poorly  
287 constrained processes, particularly those associated with the biological pump. With current  
288 trends in climate change, the size and biodiversity of phytoplankton are predicted to decrease  
289 globally<sup>42,43</sup>. Furthermore, in spite of the potential importance of viruses revealed in this  
290 study, they have largely been ignored because of limitations in sampling technologies.  
291 Consequently, as oligotrophic gyres expand and global mean NPP decreases<sup>44</sup>, the field is  
292 currently unable to predict the consequences for carbon export from the ocean's euphotic  
293 zone. By pinpointing key species that appear to be strongly associated with carbon export in

294 these areas, as well as their co-occurrences within plankton communities and key microbial  
295 functions, the integrated datasets combined with advanced computational techniques used in  
296 this study could provide a framework to address this critical bottleneck.

297 One of the grand challenges in the life sciences is to link genes to ecosystems<sup>45</sup>, based on the  
298 posit that genes can have predictable ecological footprints at community and ecosystem  
299 levels<sup>46-48</sup>. The extensive data sets from *Tara* Oceans have allowed us to predict as much as  
300 89% of the variability in carbon export from the oligotrophic surface ocean with just a small  
301 number of genes, largely with unknown functions, encoded by prokaryotes and viruses.  
302 These findings can be used as a basis to include biological complexity and guide  
303 experimental work designed to inform modeling of the global carbon cycle and to understand  
304 how it influences and is influenced by changes in climate. Such statistical analyses scaling  
305 from gene-to-ecosystems may open the way to the development of a new conceptual and  
306 methodological framework to better understand the mechanisms underpinning key ecological  
307 processes.

- 309 1 Field, C. B., Behrenfeld, M. J., Randerson, J. T. & Falkowski, P. Primary production of the biosphere:  
310 Integrating terrestrial and oceanic components. *Science* **281**, 237-240,  
311 doi:10.1126/Science.281.5374.237 (1998).
- 312 2 Boyd, P. W. & Newton, P. Evidence of the potential Influence of planktonic community structure on  
313 the interannual variability of particulate organic-carbon flux. *Deep-Sea Res. I.* **42**, 619-639 (1995).
- 314 3 Guidi, L. *et al.* Effects of phytoplankton community on production, size, and export of large  
315 aggregates: A world-ocean analysis. *Limnol. Oceanogr.* **54**, 1951-1963 (2009).
- 316 4 Kwon, E. Y., Primeau, F. & Sarmiento, J. L. The impact of remineralization depth on the air-sea  
317 carbon balance. *Nat Geosci* **2**, 630-635 (2009).
- 318 5 IPCC. *Climate Change 2013: The Physical Science Basis. Contribution of Working Group I to the*  
319 *Fifth Assessment Report of the Intergovernmental Panel on Climate Change.* (Cambridge University  
320 Press, 2013).
- 321 6 Kitano, H. Biological robustness. *Nat Rev Genet* **5**, 826-837, doi:10.1038/Nrg1471 (2004).
- 322 7 Suweis, S., Simini, F., Banavar, J. R. & Maritan, A. Emergence of structural and dynamical properties  
323 of ecological mutualistic networks. *Nature* **500**, 449-452, doi:10.1038/Nature12438 (2013).
- 324 8 Chow, C. E. T., Kim, D. Y., Sachdeva, R., Caron, D. A. & Fuhrman, J. A. Top-down controls on  
325 bacterial community structure: microbial network analysis of bacteria, T4-like viruses and protists.  
326 *ISME J.* **8**, 816-829, doi:10.1038/Ismej.2013.199 (2014).
- 327 9 Fuhrman, J. A. Microbial community structure and its functional implications. *Nature* **459**, 193-199,  
328 doi:10.1038/Nature08058 (2009).
- 329 10 Lima-Mendez, G. *et al.* Determinants of community structure in the global plankton interactome.  
330 *Science* **348**, doi:10.1126/science.1262073 (2015).
- 331 11 Giering, S. L. C. *et al.* Reconciliation of the carbon budget in the ocean's twilight zone. *Nature* **507**,  
332 480-483 (2014).
- 333 12 Azam, F. Microbial control of oceanic carbon flux: The plot thickens. *Science* **280**, 694-696 (1998).
- 334 13 Agusti, S. *et al.* Ubiquitous healthy diatoms in the deep sea confirm deep carbon injection by the  
335 biological pump. *Nat Commun* **6**, doi:10.1038/Ncomms8608 (2015).
- 336 14 Sancetta, C., Villareal, T. & Falkowski, P. Massive Fluxes of Rhizosolenid Diatoms - a Common  
337 Occurrence. *Limnol. Oceanogr.* **36**, 1452-1457 (1991).
- 338 15 Scharek, R., Tupas, L. M. & Karl, D. M. Diatom fluxes to the deep sea in the oligotrophic north  
339 Pacific gyre at station ALOHA. *Mar. Ecol. Prog. Ser.* **182**, 55-67, doi:10.3354/meps182055 (1999).
- 340 16 Omand, M. M. *et al.* Eddy-driven subduction exports particulate organic carbon from the spring  
341 bloom. *Science* **348**, 222-225, doi:10.1126/science.1260062 (2015).
- 342 17 Richardson, T. L. & Jackson, G. A. Small phytoplankton and carbon export from the surface ocean.  
343 *Science* **315**, 838-840 (2007).
- 344 18 Steinberg, D. K. *et al.* Bacterial vs. zooplankton control of sinking particle flux in the ocean's twilight  
345 zone. *Limnol. Oceanogr.* **53**, 1327-1338 (2008).
- 346 19 Turner, J. T. Zooplankton fecal pellets, marine snow, phytodetritus and the ocean's biological pump.  
347 *Prog. Oceanogr.* **130**, 205-248, doi:10.1016/j.pocean.2014.08.005 (2015).
- 348 20 Karsenti, E. *et al.* A Holistic Approach to Marine Eco-Systems Biology. *Plos Biol.* **9**,  
349 doi:10.1371/journal.pbio.1001177 (2011).
- 350 21 Strom, S. L. Microbial ecology of ocean biogeochemistry: A community perspective. *Science* **320**,  
351 1043-1045, doi:10.1126/Science.1153527 (2008).
- 352 22 Worden, A. Z. *et al.* Rethinking the marine carbon cycle: Factoring in the multifarious lifestyles of  
353 microbes. *Science* **347**, 1257594, doi:10.1126/Science.1257594 (2015).
- 354 23 Sunagawa, S. *et al.* Structure and function of the global ocean microbiome. *Science* **348**,  
355 doi:10.1126/science.1261359 (2015).
- 356 24 de Vargas, C. *et al.* Eukaryotic plankton diversity in the sunlit ocean. *Science* **348**,  
357 doi:10.1126/science.1261605 (2015).
- 358 25 Brum, J. R. *et al.* Patterns and ecological drivers of ocean viral communities. *Science* **348**,  
359 doi:10.1126/science.1261498 (2015).
- 360 26 Bork, P. *et al.* Tara Oceans studies plankton at PLANETARY SCALE. *Science* **348**, 873-873,  
361 doi:10.1126/science.aac5605 (2015).
- 362 27 Honjo, S., Manganini, S. J., Krishfield, R. A. & Francois, R. Particulate organic carbon fluxes to the  
363 ocean interior and factors controlling the biological pump: A synthesis of global sediment trap  
364 programs since 1983. *Prog. Oceanogr.* **76**, 217-285, doi:10.1016/j.pocean.2007.11.003 (2008).

365 28 Henson, S. A., Sanders, R. & Madsen, E. Global patterns in efficiency of particulate organic carbon  
366 export and transfer to the deep ocean. *Global. Biogeochem. Cy.* **26**, doi:10.1029/2011GB004099  
367 (2012).

368 29 Lê Cao, K. A., Rossouw, D., Robert-Granié, C. & Besse, P. A Sparse PLS for Variable Selection when  
369 Integrating Omics Data. *Stat Appl Genet Mol* **7**, doi:10.2202/1544-6115.1390 (2008).

370 30 Chaffron, S., Rehrauer, H., Pernthaler, J. & von Mering, C. A global network of coexisting microbes  
371 from environmental and whole-genome sequence data. *Genome Res.* **20**, 947-959,  
372 doi:10.1101/Gr.104521.109 (2010).

373 31 Faust, K. & Raes, J. Microbial interactions: from networks to models. *Nat. Rev. Microbiol.* **10**, 538-  
374 550, doi:10.1038/Nrmicro2832 (2012).

375 32 Aylward, F. O. *et al.* Microbial community transcriptional networks are conserved in three domains at  
376 ocean basin scales. *Proceedings of the National Academy of Sciences*, doi:10.1073/pnas.1502883112  
377 (2015).

378 33 Langfelder, P. & Horvath, S. WGCNA: an R package for weighted correlation network analysis. *Bmc*  
379 *Bioinformatics* **9** (2008).

380 34 Fontanez, K. M., Eppley, J. M., Samo, T. J., Karl, D. M. & DeLong, E. F. Microbial community  
381 structure and function on sinking particles in the North Pacific Subtropical Gyre. *Front Microbiol* **6**,  
382 Artn 469, doi:10.3389/Fmicb.2015.00/169 (2015).

383 35 Biard, T. *et al.* *In situ* imaging reveals the biomass of large protists in the global ocean. *Nature*  
384 (submitted).

385 36 Thomas, T. *et al.* Analysis of the *Pseudoalteromonas tunicata* Genome Reveals Properties of a  
386 Surface-Associated Life Style in the Marine Environment. *PLoS ONE* **3**,  
387 doi:10.1371/journal.pone.0003252 (2008).

388 37 Azam, F. & Malfatti, F. Microbial structuring of marine ecosystems. *Nat. Rev. Microbiol.* **5**, 782-791,  
389 doi:10.1038/nrmicro1747 (2007).

390 38 Shi, Y. M., Tyson, G. W. & DeLong, E. F. Metatranscriptomics reveals unique microbial small RNAs  
391 in the ocean's water column. *Nature* **459**, 266-U154, doi:10.1038/nature08055 (2009).

392 39 Yooshef, S. *et al.* The Sorcerer II Global Ocean Sampling expedition: Expanding the universe of  
393 protein families. *Plos Biol.* **5**, 432-466, doi:10.1371/journal.pbio.0050016 (2007).

394 40 Suttle, C. A. Marine viruses - major players in the global ecosystem. *Nat. Rev. Microbiol.* **5**, 801-812,  
395 doi:10.1038/Nrmicro1750 (2007).

396 41 Weinbauer, M. G. Ecology of prokaryotic viruses. *Fems Microbiol Rev* **28**, 127-181,  
397 doi:10.1016/j.femsre.2003.08.001 (2004).

398 42 Finkel, Z. V. *et al.* Phytoplankton in a changing world: cell size and elemental stoichiometry. *J.*  
399 *Plankton Res.* **32**, 119-137 (2010).

400 43 Sommer, U. & Lewandowska, A. Climate change and the phytoplankton spring bloom: warming and  
401 overwintering zooplankton have similar effects on phytoplankton. *Glob. Change Biol.* **17**, 154-162,  
402 doi:10.1111/J.1365-2486.2010.02182.X (2011).

403 44 Behrenfeld, M. J. *et al.* Climate-driven trends in contemporary ocean productivity. *Nature* **444**, 752-  
404 755 (2006).

405 45 DeLong, E. F. *et al.* Community genomics among stratified microbial assemblages in the ocean's  
406 interior. *Science* **311**, 496-503, doi:10.1126/Science.1120250 (2006).

407 46 Gianoulis, T. A. *et al.* Quantifying environmental adaptation of metabolic pathways in metagenomics.  
408 *P. Natl. Acad. Sci. USA* **106**, 1374-1379, doi:10.1073/Pnas.0808022106 (2009).

409 47 Tilman, D. *et al.* The influence of functional diversity and composition on ecosystem processes.  
410 *Science* **277**, 1300-1302, doi:10.1126/Science.277.5330.1300 (1997).

411 48 Wymore, A. S. *et al.* Genes to ecosystems: exploring the frontiers of ecology with one of the smallest  
412 biological units. *New Phytol* **191**, 19-36, doi:10.1111/J.1469-8137.2011.03730.X (2011).

413

414 **Figure Legends:**

415 **Figure 1 | Global view of carbon fluxes along the *Tara* Oceans circumnavigation route.**  
416 Carbon flux in  $\text{mg}\cdot\text{m}^{-2}\cdot\text{d}^{-1}$  estimated from particles size distribution and abundance measured  
417 with the Underwater Vision Profiler 5 (UVP5).

418  
419 **Figure 2 | Eukaryotic community associated to carbon export seen using standard**  
420 **methods for regression-based modeling of high dimensional data.** Eukaryotic lineages  
421 associated to carbon export as revealed by sPLS analysis. Correlations between lineages and  
422 environmental parameters are depicted as a clustered heatmap and lineages with a correlation  
423 to carbon export higher than 0.2 are highlighted.

424  
425 **Figure 3 | Ecological networks reveal key taxa lineages associated with carbon export at**  
426 **global scale.** The relative abundances of taxa in selected subnetworks were used to estimate  
427 carbon export and to identify key lineages associated with the process. **a**, The selected  
428 eukaryotic subnetwork ( $n=49$ , see Supplementary Information SI2) can predict carbon export  
429 with high accuracy (PLS regression, LOOCV,  $R^2=0.69$ , see Extended data Fig. 3a). Lineages  
430 with the highest VIP score (dots size is proportional to the VIP score in the scatter plot) in  
431 the PLS are depicted as red dots corresponding to three Rhizaria (Collodaria, *Collozoum*  
432 *inerme* and *Sticholonche* sp.), one copepod (*Oithona* sp.), one siphonophore (*Lilyopsis*),  
433 three Dinophyceae and one ciliate (*Spirotontonia turbinata*). **b**, The selected prokaryotic  
434 subnetwork ( $n=109$ , see Supplementary Information SI3) can predict carbon export with  
435 good accuracy (PLS regression, LOOCV,  $R^2=0.60$ , see Extended data Fig. 3b). **c**, The  
436 selected viral population subnetwork ( $n=277$ , see Supplementary Information SI4) can  
437 predict carbon export with high accuracy (PLS regression, LOOCV,  $R^2=0.89$ , see Extended  
438 data Fig. 3c). Two viral populations with a high VIP score (red dots) are predicted as  
439 *Synechococcus* phages (see Supplementary Information SI4).

440 **Figure 4 | Plankton community network built from eukaryotic, prokaryotic and viral**  
441 **subnetworks related to carbon export.** Major lineages were selected within the three  
442 subnetworks ( $\text{VIP} > 1$ ). Co-occurrences between all lineages of interest were extracted from  
443 a previously established global co-occurrence network (see methods). Only lineages  
444 discussed within the study are pinpointed. The resulting graph is composed of 329 nodes,  
445 467 edges, with a diameter of 7, and average weighted degree of 4.6.

446 **Figure 5 | Bacterial functional networks reveal key functions associated with carbon**  
447 **export at global scale.** A bacterial functional network was built based on Orthologous  
448 Group/Gene (OG) relative abundances using the WGCNA methodology (see Methods) and  
449 correlated to classical oceanographic parameters. **a**, Two functional subnetworks (light and  
450 dark green, FNET1 ( $n=220$ ) and FNET2 ( $n=441$ ), respectively) are significantly associated  
451 with carbon export (FNET1: Pearson cor. 0.42,  $p = 4e^{-09}$  and FNET2: 0.54,  $p = 7e^{-06}$ , see  
452 Extended data Fig. 5a). The highest VIP score functions from top to bottom correspond to  
453 red dots from right to left. **b**, Higher functional categories are depicted for functions with a  
454 VIP score  $>1$  (PLS regression, LOOCV, FNET1  $R^2=0.41$  and FNET2  $R^2=0.48$ , see Extended  
455 data Fig. 6) in both functional subnetworks,



## 456 **Methods**

### 457 **Environmental data collection**

458 From 2009-2013, environmental data (Supplementary Information SI9) were collected across all  
459 major oceanic provinces in the context of the *Tara* Oceans expeditions<sup>20</sup>. Sampling stations were  
460 selected to represent distinct marine ecosystems at a global scale<sup>49</sup>. Note that Southern Ocean stations  
461 were not examined herein because they were ranked as outliers due to their exceptional  
462 environmental characteristics and biota<sup>23,24</sup>. Environmental data were obtained from vertical profiles  
463 of a sampling package<sup>50,51</sup>. It consisted of conductivity and temperature sensors, chlorophyll and  
464 CDOM fluorometers, light transmissometer (Wetlabs C-star 25cm), a backscatter sensor (WetLabs  
465 ECO BB), a nitrate sensor (SATLANTIC ISUS) and a Hydroptic Underwater Vision Profiler (UVP;  
466 Hydroptics<sup>52</sup>. Nitrate and fluorescence to chlorophyll concentrations as well as salinity were  
467 calibrated from water samples collected with Niskin bottle<sup>50</sup>. Net Primary Production (NPP) data  
468 were extracted from 8 day composites of the Vertically Generalized Production Model (VGPM<sup>53</sup>) at  
469 the week of sampling<sup>54</sup>. Carbon fluxes and carbon export, corresponding to the carbon flux at 150 m,  
470 were estimated based on particle concentration and size distributions obtained from the UVP<sup>51</sup> and  
471 details are presented below.

### 472 **From particle size distribution to carbon export estimation**

473 Previous research has shown that the distribution of particle size follows a power law over the  $\mu\text{m}$  to  
474 the mm size range<sup>3,55,56</sup>. This *Junge*-type distribution translates into the following mathematical  
475 equation, whose parameters can be retrieved from UVP images:

$$n(d) = ad^k \quad (\text{eq. 1})$$

476 where  $d$  is the particle diameter, and exponent  $k$  is defined as the slope of the number spectrum when  
477 equation (2) is log transformed. This slope is commonly used as a descriptor of the shape of the  
478 aggregate size distribution.  
479

480  
481 The carbon-based particle size approach relies on the assumption that the total carbon flux of  
482 particles ( $F$ ) corresponds to the flux spectrum integrated over all particle sizes:

$$F = \int_0^{\infty} n(d) \cdot m(d) \cdot w(d) dd \quad (\text{eq. 2})$$

483 where  $n(d)$  is the particle size spectrum, i.e., equation (1), and  $m(d)$  is the mass (here carbon content)  
484 of a spherical particle described as:

$$m(d) = \alpha d^3 \quad (\text{eq. 3})$$

485 where  $\alpha = \pi\rho/6$ ,  $\rho$  is the average density of the particle, and  $w(d)$  is the settling rate calculated using  
486 Stokes Law:

$$w(d) = \beta d^2 \quad (\text{eq. 4})$$

487 where  $\beta = g(\rho - \rho_0)(18\nu\rho_0)^{-1}$ ,  $g$  is the gravitational acceleration,  $\rho_0$  the fluid density, and  $\nu$  the  
488 kinematic viscosity.

489  
490 In addition, mass and settling rates of particles,  $m(d)$  and  $w(d)$ , respectively, are often described as  
491 power law functions of their diameter obtained by fitting observed data,  $m(d) \cdot w(d) = Ad^B$ . The

492 particles carbon flux can then be estimated using an approximation of Eq. 2 over a finite number ( $x$ )  
493 of small logarithmic intervals for diameter  $d$  spanning from 250  $\mu\text{m}$  to 1.5 mm (particles  $<250 \mu\text{m}$   
494 and  $>1.5 \text{ mm}$  are not considered, consistent with the method presented by *Guidi et al., [2008]<sup>57</sup>*) such  
495 as

$$F = \sum_{i=1}^x n_i A d_i^B \Delta d_i \quad (\text{eq. 5})$$

496

497 where  $A=12.5\pm 3.40$  and  $B=3.81 \pm 0.70$  have been estimated using a global dataset that compared  
498 particle fluxes in sediment traps and particle size distributions from the UVP images.

#### 499 **Genomic data collection**

500 For the sake of consistency between all available datasets from the *Tara* Oceans expeditions, we  
501 considered subsets of the data recently published in *Science*<sup>23-25</sup>. In brief, one sample corresponds to  
502 data collected at one depth (surface (SRF) or Deep Chlorophyll Maximum (DCM) determined from  
503 the profile of chlorophyll fluorometer) and at one station. To study the eukaryotic community in our  
504 current manuscript, we selected stations at which we had environmental data and carbon export  
505 estimated at 150 m with the UVP and all size fractions. Consequently a subset of 33 stations  
506 (corresponding to 56 samples) has been created compared to the 47 stations analyzed in *de Vargas et*  
507 *al. [2015]*. A similar procedure has been applied to the prokaryotic and viral datasets, reducing the  
508 *Sunagawa et al. [2015]* prokaryotic dataset to a subset of 104 samples from 62 stations and the *Brum*  
509 *et al. [2015]* viral dataset into a subset of 37 samples from 22 stations (See Supplementary  
510 Information SI10). In addition a detailed table is provided summarizing which samples (depth and  
511 station) are available for each domain (Supplementary Information SI11).

#### 512 **Eukaryotic taxa profiling**

513 Photic-zone eukaryotic plankton diversity has been investigated through millions of environmental  
514 Illumina reads. Sequences of the 18S ribosomal RNA gene V9 region were obtained by PCR  
515 amplification and a stringent quality-check pipeline has been applied to remove potential chimera or  
516 rare sequences (details on data cleaning in *de Vargas et al. [2015]<sup>24</sup>*). For 47 stations, and if possible  
517 at two depths (SRF and DCM), eukaryotic communities were sampled in the *piconano-* (0.8-5  $\mu\text{m}$ ),  
518 *micro-* (20-180  $\mu\text{m}$ ) and *meso-*plankton (180-2000  $\mu\text{m}$ ) fractions (a detailed list of these samples is  
519 given in Supplementary Information SI12). In the framework of the carbon export study, sequences  
520 from all size fractions were pooled in order to get the most accurate and statistically reliable dataset  
521 of the eukaryotic community. The 2.3 million eukaryotic ribotypes were assigned to known  
522 eukaryotic taxonomic entities by global alignment to a curated database<sup>24</sup>. To get the most accurate  
523 vision of the eukaryotic community, sequences showing less than 97% identity with reference  
524 sequences were excluded. The final eukaryotic relative abundance matrix used in our analyses  
525 included 1,750 lineages (taxonomic assignment has been performed using a last common ancestor  
526 methodology, and had thus been performed down to species level when possible) in 56 samples from  
527 33 stations. Pooled abundance (number of V9 sequences) of each lineage has been normalized by the  
528 total sum of sequences in each sample.

#### 529 **Prokaryotic taxa profiling**

530 To investigate the prokaryotic lineages, communities were sampled in the pico-plankton. Both filter  
531 sizes have been used along the *Tara* Oceans transect: up to station #52, prokaryotic fractions  
532 correspond to a 0.22-1.6  $\mu\text{m}$  size fraction, and from station #56, prokaryotic fractions correspond to a

533 0.22-3  $\mu\text{m}$  size fraction. Prokaryotic taxonomic profiling was performed using 16S rRNA gene tags  
534 directly identified in Illumina-sequenced metagenomes ( $_{\text{mi}}\text{tags}$ ) as described in *Logares et al.*,  
535 [2014]<sup>58</sup>. 16S  $_{\text{mi}}\text{tags}$  were mapped to cluster centroids of taxonomically annotated 16S reference  
536 sequences from the SILVA database<sup>59</sup> (release 115: SSU Ref NR 99) that had been clustered at 97%  
537 sequence identity using USEARCH v6.0.307<sup>60</sup>. 16S  $_{\text{mi}}\text{tag}$  counts were normalized by the total reads  
538 count in each sample (further details in *Sunagawa et al.* [2015]<sup>23</sup>). The photic-zone prokaryotic  
539 relative abundance matrix used in our analyses included 3,253,962  $_{\text{mi}}\text{tags}$  corresponding to 1,328  
540 genera in 104 samples from 62 stations.

541

#### 542 **Prokaryotic functional profiling**

543 For each prokaryotic sample, gene relative abundance profiles were generated by mapping reads to  
544 the OM-RGC using the MOCAT pipeline<sup>61</sup>. The relative abundance of each reference gene was  
545 calculated as gene length-normalized base counts. And functional abundances were calculated as the  
546 sum of the relative abundances of these reference genes, annotated to OG functional groups. In our  
547 analyses, we used the subset of the OM-RGC that was annotated to Bacteria or Archaea (24.4 M  
548 genes). Using a rarefied (to 33 M inserts) gene count table, an OG was considered to be part of the  
549 ocean microbial core if at least one insert from each sample was mapped to a gene annotated to that  
550 OG. For further details on the prokaryotic profiling please refer to *Sunagawa et al.* [2015]<sup>23</sup>. The final  
551 prokaryotic functional relative abundance matrix used in our analyses included 37,832 OGs or  
552 functions in 104 samples from 62 stations. Genes from functions of FNET1 and FNET2 subnetworks  
553 were taxonomically annotated using a modified dual BLAST-based last common ancestor (2bLCA)  
554 approach<sup>62</sup>. We used RAPsearch2<sup>63</sup> rather than BLAST to efficiently process the large data volume  
555 and a database of non-redundant protein sequences from UniProt (version: UniRef\_2013\_07) and  
556 eukaryotic transcriptome data not represented in UniRef (see Supplementary Information SI5, SI6,  
557 for full annotations).

#### 558 **Enumeration of prokaryotes by flow cytometry**

559 For prokaryote enumeration by flow cytometry, three aliquots of 1 ml of seawater (pre-filtered by  
560 200- $\mu\text{m}$  mesh) were collected from both SRF and DCM. The samples were fixed immediately using  
561 cold 25% glutaraldehyde (final concentration 0.125%), left in the dark for 10 min at room  
562 temperature, flash-frozen and kept in liquid nitrogen on board and then stored at -80°C on land. Two  
563 subsamples were taken to separate counts of heterotrophic prokaryotes (not shown herein) and  
564 phototrophic picoplankton. For heterotrophic prokaryote determination, 400  $\mu\text{l}$  of sample was added  
565 to a diluted SYTO-13 (Molecular Probes Inc., Eugene, OR, USA) stock (10:1) at 2.5  $\mu\text{mol l}^{-1}$  final  
566 concentration, left for about 10 min in the dark to complete the staining and run in the flow  
567 cytometer. We used a FacsCalibur (Becton & Dickinson) flow cytometer equipped with a 15 mW  
568 Argon-ion laser (488 nm emission). At least 30,000 events were acquired for each subsample (usually  
569 100,000 events). Fluorescent beads (1  $\mu\text{m}$ , Fluoresbrite carboxylate microspheres, Polysciences Inc.,  
570 Warrington, PA) were added at a known density as internal standards. The bead standard  
571 concentration was determined by epifluorescence microscopy. For phototrophic picoplankton, we  
572 used the same procedure as for heterotrophic prokaryote, but without addition of SYTO-13. Data  
573 analysis was performed with FlowJo software (Tree Star, Inc.).

#### 574 **Profiling of viral populations**

575 In order to associate viruses to carbon export we used viral populations as defined in *Brum et al.*  
576 [2015]<sup>25</sup> using a set of 43 *Tara* Oceans viromes. Briefly, viral populations were defined as large  
577 contigs (>10 predicted genes and >10 kb) identified as most likely originating from bacterial or  
578 archaeal viruses. These 6,322 contigs remained and were then clustered into populations if they

579 shared more than 80% of their genes at >95% nucleotide identity. This resulted in 5,477  
580 ‘populations’ from the 6,322 contigs, where as many as 12 contigs were included per population. For  
581 each population, the longest contig was chosen as the ‘seed’ representative sequence. The relative  
582 abundance of each population was computed by mapping all quality-controlled reads to the set of  
583 5,477 non-redundant populations (considering only mapping quality scores greater than 1) with  
584 Bowtie2<sup>64</sup> and if more than 75% of the reference sequence was covered by virome reads. The relative  
585 abundance of a population in a sample was computed as the number of base pairs recruited to the  
586 contig normalized to the total number of base pairs available in the virome and the contig length if  
587 more than 75% of the reference sequence was covered by virome reads, and set to 0 otherwise (see  
588 *Brum et al.* [2015]<sup>25</sup> for further details). The final viral population abundance matrix used in our  
589 analyses included 5,291 viral population contigs in 37 samples from 22 stations.

### 590 **Viral host predictions**

591 The longest contig in a population was defined as the seed sequence and considered the best estimate  
592 of that population’s origin. These seed sequences were used to assess taxonomic affiliation of each  
593 viral population. Cases where >50% of the genes were affiliated to a specific reference genome from  
594 RefSeq Virus (based on a BLASTp comparison with thresholds of 50 for bit score and 10<sup>-5</sup> for e-  
595 value) with an identity percentage of at least 75% (at the protein sequence level) were considered as  
596 confident affiliations to the corresponding reference virus. The viral population host group was then  
597 estimated based on these confident affiliations (see Supplementary Information SI13 for host  
598 affiliation of viral population contigs associated to carbon export).

### 599 **Viral protein clusters**

600 Viral protein clusters (PCs) correspond to ORFs initially mapped to existing clusters (POV, GOS and  
601 phage genomes). The remaining, unmapped ORFs were self-clustered, using cd-hit as described in  
602 *Brum et al.* [2015]<sup>25</sup>. Only PCs with more than two ORFs were considered bona fide and were used  
603 for subsequent analyses. To compute PC relative abundance for statistical analyses, reads were  
604 mapped back to predicted ORFs in the contigs dataset using Mosaik as described in *Brum et al.*  
605 [2015]<sup>25</sup>. Read counts to PCs were normalized by sequencing depth of each virome. Importantly, we  
606 restricted our analyses to 4,294 PCs associated to the 277 viral population contigs significantly  
607 associated to carbon export in 37 samples from 22 stations.

### 608 **Sparse Partial Least Squares analysis**

609 In order to directly associate eukaryotic lineages to carbon export and other environmental traits (Fig.  
610 2), we used sparse Partial Least Square (sPLS<sup>65</sup> as implemented in the R package *mixOmics*<sup>29</sup>. We  
611 applied the sPLS in regression mode, which will model a causal relationship between the lineages  
612 and the environmental traits, *i.e.* PLS will predict environmental traits (*e.g.* carbon export) from  
613 lineage abundances. This approach enabled us to identify high correlations (see Supplementary  
614 Information SI1) between certain lineages and carbon export but without taking into account the  
615 global structure of the planktonic community.

### 616 **Co-occurrence network model analysis**

617 Weighted correlation network analysis (WGCNA) was performed to delineate feature (lineages, viral  
618 populations, PCs or functions) subnetworks based on their relative abundance<sup>66,67</sup>. A signed  
619 adjacency measure for each pair of features was calculated by raising the absolute value of their  
620 Pearson correlation coefficient to the power of a parameter *p*. The default value *p*=6 was used for  
621 each global network, except for the Prokaryotic functional network where *p* had to be lowered to 4 in  
622 order to optimize the scale-free topology network fit. Indeed, this power allows the weighted

623 correlation network to show a scale free topology where key nodes are highly connected with others.  
624 The obtained adjacency matrix was then used to calculate the topological overlap measure (TOM),  
625 which for each pair of features, taking into account their weighted pairwise correlation (direct  
626 relationships) and their weighted correlations with other features in the network (indirect  
627 relationships). For identifying subnetworks a hierarchical clustering was performed using a distance  
628 based on the TOM measure. This resulted in the definition of several subnetworks, each represented  
629 by its first principal component.

630 These characteristic components play a key role in weighted correlation network analysis. On the one  
631 hand, the closeness of each feature to its cluster, referred to as the subnetwork membership, is  
632 measured by correlating its relative abundance with the first principal component of the subnetwork.  
633 On the other hand, association between the subnetworks and a given trait is measured by the pairwise  
634 Pearson correlation coefficients between the considered environmental trait and their respective  
635 principal components. A similar protocol has been performed on the eukaryotic relative abundance  
636 matrix, the prokaryotic relative abundance matrix, the prokaryotic functions relative abundance  
637 matrix and the viral population and PC relative abundance matrices. All procedures were applied on  
638 Hellinger-transformed log-scaled abundances. Noteworthy, the protocol is not sensitive to copy  
639 number variation as observed across different eukaryotic species, because the association between  
640 two species relies on a correlation score between relative abundance measurements. Computations  
641 were carried out using the R package *WGCNA*<sup>33</sup>.

642 Given the nature of the eukaryotic dataset (three distinct size fractions), the sampling process may  
643 lead to the loss of size fractions. In particular, samples #1, #3, #17, #37, #39, #43, #48, #53, #54, #55,  
644 #66 are eventually biases by such a loss (Supplementary Information SI12). A complementary  
645 WGCNA analysis was performed with addition of these samples to evaluate the robustness of our  
646 protocol to missing size fractions. The composition of the eukaryotic subnetwork built with an  
647 extended dataset (*i.e.*, 67 samples from 37 stations for which size fractions were missing in 11  
648 samples) was compared to the subnetwork as presented above (*i.e.*, 56 samples from 33 stations).  
649 Both subnetworks shown an overlap of 75% of lineage, whereas four of the top five VIP lineages  
650 with the extended dataset (see Extended data Fig. 8 for details) can be found in the top six VIP  
651 lineages of the above subnetwork (Supplementary Information SI2), emphasizing highly similar  
652 results and a small sensitivity to size fraction loss.

### 653 **Extraction of subnetworks related to carbon export**

654 For each subnetwork (called modules within WGCNA) extracted from each global network, pairwise  
655 Pearson correlation coefficients between the subnetwork principal components and the carbon export  
656 estimation was computed, as well as corresponding p-values corrected for multiple testing using the  
657 Benjamini & Hochberg FDR procedure. The subnetworks showing the highest correlation scores are  
658 of interest and were investigated. One subnetwork (49 nodes) was significant within the eukaryotic  
659 network; one subnetwork (109 nodes) was significant for the prokaryotic network; one subnetwork  
660 (277 nodes) was significant within the virus network; two subnetworks (441 and 220 nodes) were  
661 significant within the prokaryotic functional network, and two subnetworks (1,879 and 2,147 nodes)  
662 were significant within the viral PCs network.

### 663 **Partial Least Squares regression**

664 In addition to the network analyses, we asked whether the identified subnetworks can be used as  
665 predictors for the carbon export estimations. To answer this question, we used Partial least squares  
666 (PLS) regression, which is a dimensionality-reduction method that aims at determining predictor

667 combinations with maximum covariance with the response variable. The identified combinations,  
668 called latent variables, are used to predict the response variable. The predictive power of the model is  
669 assessed by correlating the predicted vector with the measured values. The significance of the  
670 prediction power was evaluated by permuting the data 10,000 times. For each permutation, a PLS  
671 model was built to predict the randomized response variable and a Pearson correlation was calculated  
672 between the permuted response variable and in Leave-One-Out Cross-Validation (LOOCV) predicted  
673 values. The 10,000 random correlations are compared to the performance of the PLS model that were  
674 used to predict the true response variable. In addition, the predictors were ranked according to their  
675 value importance in projection (VIP)<sup>68</sup>. The VIP measure of a predictor estimates its contribution in  
676 the PLS regression. The predictors having high VIP values are assumed important for the PLS  
677 prediction of the response variable. The VIP values of the prokaryotic functional subnetworks are  
678 provided in Supplementary Information SI5, SI6. For the sake of illustration, only lineages or  
679 functions with  $VIP > 1^{68}$  are discussed and pictured in Figure 4 and 5. Our computations were carried  
680 out using the R package pls<sup>69</sup>. All programs are available under GPL Licence.

### 681 **Subnetwork representations**

682 Nodes of the subnetworks represent either lineages (eukaryotic, prokaryotic or viral) or functions  
683 (prokaryotic or viral). Subnetworks related to the carbon export have been represented in two distinct  
684 formats. Scatter plots represent each nodes based on their Pearson correlation to the carbon export  
685 and their respective node centrality within the subnetwork. The latter has been recomputed using  
686 significant Spearman correlations above 0.3 (>0.9 for viral PCs) as edges, this is done for  
687 visualization purposes since WGCNA subnetworks (based on the Topology Overlap Measure (TOM)  
688 between nodes) are hyper-connected. Size representation of nodes are proportional to the VIP score  
689 after PLS. The hiveplots depict the same subnetworks by focusing on two main features: x-axis and  
690 y-axis depict nodes of subnetworks ranked by their VIP scores and Pearson correlation to the carbon  
691 export, respectively.

### 692 **References and Notes (Methods)**

- 693 49 Pesant, S. *et al.* Open science resources for the discovery and analysis of Tara Oceans data. *Scientific*  
694 *Data* **2**, 150023, doi:10.1038/sdata.2015.23 (2015).
- 695 50 Picheral, M. *et al.* Vertical profiles of environmental parameters measured on discrete water samples  
696 collected with Niskin bottles during the Tara Oceans expedition 2009-2013.  
697 doi:10.1594/PANGAEA.836319 (2014).
- 698 51 Picheral, M. *et al.* Vertical profiles of environmental parameters measured from physical, optical and  
699 imaging sensors during Tara Oceans expedition 2009-2013. doi:10.1594/PANGAEA.836321 (2014).
- 700 52 Picheral, M. *et al.* The Underwater Vision Profiler 5: An advanced instrument for high spatial  
701 resolution studies of particle size spectra and zooplankton. *Limnol. Oceanogr. Meth.* **8**, 462–473,  
702 doi:10.4319/lom.2010.8.462 (2010).
- 703 53 Behrenfeld, M. J. & Falkowski, P. G. Photosynthetic rates derived from satellite-based chlorophyll  
704 concentration. *Limnol. Oceanogr.* **42**, 1-20 (1997).
- 705 54 Chaffron, S. *et al.* Contextual environmental data of selected samples from the Tara Oceans  
706 Expedition (2009-2013). doi:10.1594/PANGAEA.840718 (2014).
- 707 55 McCave, I. N. Size spectra and aggregation of suspended particles in the deep ocean. *Deep-Sea Res. I.*  
708 **31**, 329-352 (1984).
- 709 56 Sheldon, R. W., Prakash, A. & Sutcliffe, W. H. Size distribution of particles in ocean. *Limnol.*  
710 *Oceanogr.* **17**, 327-340 (1972).
- 711 57 Guidi, L. *et al.* Relationship between particle size distribution and flux in the mesopelagic zone. *Deep-*  
712 *Sea Res. I.* **55**, 1364-1374, doi:10.1016/j.dsr.2008.05.014 (2008).
- 713 58 Logares, R. *et al.* Metagenomic 16S rDNA Illumina tags are a powerful alternative to amplicon  
714 sequencing to explore diversity and structure of microbial communities. *Environ Microbiol* **16**, 2659-  
715 2671, doi:Doi 10.1111/1462-2920.12250 (2014).
- 716 59 Quast, C. *et al.* The SILVA ribosomal RNA gene database project: improved data processing and web-  
717 based tools. *Nucleic Acids Res* **41**, D590-D596, doi:10.1093/Nar/Gks1219 (2013).

- 718 60 Edgar, R. C. Search and clustering orders of magnitude faster than BLAST. *Bioinformatics* **26**, 2460-  
719 2461, doi:10.1093/Bioinformatics/Btq461 (2010).
- 720 61 Kultima, J. R. *et al.* MOCAT: A Metagenomics Assembly and Gene Prediction Toolkit. *PLoS ONE* **7**,  
721 ARTN e47656, doi:10.1371/journal.pone.0047656 (2012).
- 722 62 Hingamp, P. *et al.* Exploring nucleo-cytoplasmic large DNA viruses in Tara Oceans microbial  
723 metagenomes. *ISME J.* **7**, 1678-1695, doi:10.1038/Ismej.2013.59 (2013).
- 724 63 Zhao, Y. A., Tang, H. X. & Ye, Y. Z. RAPSearch2: a fast and memory-efficient protein similarity  
725 search tool for next-generation sequencing data. *Bioinformatics* **28**, 125-126,  
726 doi:10.1093/Bioinformatics/Btr595 (2012).
- 727 64 Langmead, B. & Salzberg, S. L. Fast gapped-read alignment with Bowtie 2. *Nat Methods* **9**, 357-  
728 U354, doi:10.1038/Nmeth.1923 (2012).
- 729 65 Shen, H. P. & Huang, J. H. Z. Sparse principal component analysis via regularized low rank matrix  
730 approximation. *J Multivariate Anal* **99**, 1015-1034, doi:10.1016/J.Jmva.2007.06.007 (2008).
- 731 66 Langfelder, P. & Horvath, S. Eigengene networks for studying the relationships between co-  
732 expression modules. *Bmc Syst Biol* **1**, Artn 54, doi:10.1186/1752-0509-1-54 (2007).
- 733 67 Li, A. & Horvath, S. Network neighborhood analysis with the multi-node topological overlap measure.  
734 *Bioinformatics* **23**, 222-231, doi:10.1093/Bioinformatics/Btl581 (2007).
- 735 68 Chong, I. G. & Jun, C. H. Performance of some variable selection methods when multicollinearity is  
736 present. *Chemometr. Intell. Lab.* **78**, 103-112, doi:10.1016/J.Chemolab.2004.12.011 (2005).
- 737 69 Mevik, B. H. & Wehrens, R. The pls package: Principal component and partial least squares  
738 regression in R. *J Stat Softw* **18**, 1-23 (2007).
- 739

## 740 Acknowledgements

741 We thank the commitment of the following people and sponsors: CNRS (in particular Groupement de  
742 Recherche GDR3280), European Molecular Biology Laboratory (EMBL), Genoscope/CEA, VIB, Stazione  
743 Zoologica Anton Dohrn, UNIMIB, Fund for Scientific Research – Flanders, Rega Institute, KU Leuven, The  
744 French Ministry of Research, the French Government 'Investissements d'Avenir' programmes OCEANOMICS  
745 (ANR-11-BTBR-0008), FRANCE GENOMIQUE (ANR-10-INBS-09-08), MEMO LIFE (ANR-10-LABX-54),  
746 PSL\* Research University (ANR-11-IDEX-0001-02), ANR (projects POSEIDON/ANR-09-BLAN-0348,  
747 PHYTBACK/ANR-2010-1709-01, PROMETHEUS/ANR-09-PCS-GENM-217, TARA-GIRUS/ANR-09-PCS-  
748 GENM-218, SAMOSA, ANR-13-ADAP-0010), European Union FP7 (MicroB3/No.287589, IHMS/HEALTH-  
749 F4-2010-261376), ERC Advanced Grant Award to CB (Diatomite: 294823), Gordon and Betty Moore  
750 Foundation grant (#3790 and #2631) and the UA Technology and Research Initiative Fund and the Water,  
751 Environmental, and Energy Solutions Initiative to MBS, Spanish Ministry of Science and Innovation grant  
752 CGL2011-26848/BOS MicroOcean PANGENOMICS to SGA, TANIT (CONES 2010-0036) from the Agència  
753 de Gestió d'Ajuts Universitaris i Reserca to SGA, JSPS KAKENHI Grant Number 26430184 to HO, and  
754 FWO, BIO5, Biosphere 2 to MBS. We also thank the support and commitment of Agnès b. and Etienne  
755 Bourgois, the Veolia Environment Foundation, Region Bretagne, Lorient Agglomeration, World Courier,  
756 Illumina, the EDF Foundation, FRB, the Prince Albert II de Monaco Foundation, the Tara schooner and its  
757 captains and crew. We thank MERCATOR-CORISOLIS and ACRI-ST for providing daily satellite data during  
758 the expedition. We are also grateful to the French Ministry of Foreign Affairs for supporting the expedition and  
759 to the countries who graciously granted sampling permissions. Tara Oceans would not exist without continuous  
760 support from 23 institutes (<http://oceans.taraexpeditions.org>). The authors further declare that all data reported  
761 herein are fully and freely available from the date of publication, with no restrictions, and that all of the  
762 samples, analyses, publications, and ownership of data are free from legal entanglement or restriction of any  
763 sort by the various nations whose waters the *Tara Oceans* expedition sampled in. This article is contribution  
764 number ZZZ of *Tara Oceans*.

## 765 Author Contributions

766 L.G., S.C., Lu.B. and D.E. designed the study and wrote the paper. C.D., M.P., J.P. and Sa.S. collected *Tara*  
767 *Oceans* samples. S.K-L managed the logistics of the *Tara Oceans* project. L.G. and M.P. analysed  
768 oceanographic data. S.C. and Lu.B. analysed taxonomic data. S.C., Lu.B., D.E. and S.R. performed the

769 genomic and statistical analyses. A.L., Y.D., L.G., S.C., Lu.B. and D.E. produced and analysed the networks.  
770 E.K., C.B. and G.G. supervised the study. M.S., J.R., E.K., C.B. and G.G. provided constructive comments,  
771 revised and edited the manuscript. *Tara* Oceans coordinators provided a creative environment and constructive  
772 criticism throughout the study. All authors discussed the results and commented on the manuscript.

### 773 **Author Information**

774 Data described herein is available at EBI under the project identifiers PRJEB402, PRJEB6610 and PRJEB7988,  
775 PANGAEA<sup>50,51,54</sup>, and a companion website (<http://www.raeslab.org/companion/ocean-carbon-export.html>).  
776 The data release policy regarding future public release of *Tara* Oceans data is described in *Pesant et al.*,  
777 [2015]<sup>49</sup>. All authors approved the final manuscript. Reprints and permissions information is available at  
778 [www.nature.com/reprints](http://www.nature.com/reprints). The authors declare no competing financial interests. Correspondence and requests  
779 for materials should be addressed to [lguidi@obs-vlfr.fr](mailto:lguidi@obs-vlfr.fr), [samuel.chaffron@vib-kuleuven.be](mailto:samuel.chaffron@vib-kuleuven.be),  
780 [lucie.bittner@upmc.fr](mailto:lucie.bittner@upmc.fr), [damien.eveillard@univ-nantes.fr](mailto:damien.eveillard@univ-nantes.fr), [Jeroen.Raes@vib-kuleuven.be](mailto:Jeroen.Raes@vib-kuleuven.be), [karsenti@embl.de](mailto:karsenti@embl.de),  
781 [cbowler@biologie.ens.fr](mailto:cbowler@biologie.ens.fr), [gorsky@obs-vlfr.fr](mailto:gorsky@obs-vlfr.fr)



782 **Extended data legends:**

783 **Extended Data Figure 1:** Overview of analytical methods used in the manuscript. **a,** Depiction of a  
784 standard pairwise analysis that considers a sequence relative abundance matrix for  $s$  samples ( $s \times$   
785 OTUs (Operational Taxonomic Units)) and its corresponding environmental matrix ( $s \times p$   
786 (parameters)). sPLS results emphasize OTU(s) that are the most correlated to environmental  
787 parameters. **b,** Depiction of a graph-based approach. Using only a relative abundance matrix ( $s \times$   
788 OTUs), WGCNA builds a graph where nodes are OTUs and edges represent significant co-  
789 occurrence. Co-occurrence scores between nodes are weights allocated to corresponding edges.  
790 These weights are magnified by a power-law function until the graph becomes scale-free. The graph  
791 is then decomposed within subnetworks (groups of OTUs) that are analyzed separately. One  
792 subnetwork (group of OTUs) is considered of interest when its topology is related to the trait of  
793 interest; in the current case carbon export. For each subnetwork (for instance the subnetwork related  
794 to carbon export), each OTU is spread within a feature space that plots each OTU based on its  
795 membership to the subnetwork ( $x$ -axis) and its correlation to the environmental trait of interest (i.e.,  
796 carbon export). A good regression of all OTUs emphasizes the putative relation of the subnetwork  
797 topology and the carbon export trait (i.e. the more a given OTU defines the subnetwork topology, the  
798 more it is correlated to carbon export). **c,** Depiction of the machine learning (PLS) approach that was  
799 applied following subnetwork identification and selection. Greater VIP scores (i.e. larger circles)  
800 emphasized most important OTUs. VIP refers to Variable Importance in Projection and reflects the  
801 relative predictive power of a given OTU. OTUs with VIP score greater than one are considered as  
802 important in the predictive model and their selection do not alter the overall predictive power.  
803

804 **Extended Data Figure 2:** Domain-specific ecological subnetworks associated to environmental  
805 parameters and species subnetwork structures correlate to carbon export. **a,b,c,** Global ecological  
806 networks were built for the 3 domains of life using the WGCNA methodology (see methods) and  
807 correlated to classical oceanographic parameters as well as carbon export (estimated at 150 m from  
808 particles size distribution and abundance). Each domain-specific global network is decomposed into  
809 smaller coherent subnetworks (depicted by distinct colours on the  $y$ -axis) and their eigen vector is  
810 correlated to all environmental parameters. Similar to a correlation at the network scale, this approach  
811 directly links subnetworks to environmental parameters (i.e. the more the taxa contribute to the  
812 subnetwork structure, the more their abundance are correlated to the parameter). The measure allows  
813 to identify subnetworks for which the overall structure is related to the carbon export. **a,** A single  
814 eukaryotic subnetwork ( $n=58$ ,  $N=1'870$ ) is strongly associated to carbon export (Pearson cor. 0.81,  $p$   
815  $= 5e^{-15}$ ). **b,** A single prokaryotic subnetwork ( $n=109$ ,  $N=1'527$ ) is moderately associated to carbon  
816 export (Pearson cor. 0.32,  $p = 9e^{-03}$ ). **c,** A single viral subnetwork ( $n=277$ ,  $N=5'476$ ) is strongly  
817 associated to carbon export (Pearson cor. 0.93,  $p = 2e^{-15}$ ). **d,e,f,** The WGCNA approach directly links  
818 subnetworks to environmental parameters, i.e. the more the features contribute to the subnetwork  
819 structure (topology), the more their abundance are correlated to the parameter. This measure allows  
820 to identify subnetworks for which the overall structure, summarized as the eigen vector of the  
821 subnetwork, is related to the carbon export. **d,** The eukaryotic subnetwork structure correlates to  
822 carbon export (Pearson cor. = 0.87,  $p = 5e^{-16}$ ). **e,** The prokaryotic subnetwork structure correlates to  
823 carbon export (Pearson cor. = 0.47,  $p = 5e^{-06}$ ). **f,** The viral population subnetwork structure correlates  
824 to carbon export (Pearson cor. = 0.88,  $p = 6e^{-93}$ ).  
825

826 **Extended Data Figure 3:** Species subnetworks predict carbon export. PLS regression was used to  
827 predict carbon export using lineage abundances in selected subnetworks. LOOCV was performed and  
828 VIP scores computed for each lineage. **a,** The eukaryotic subnetwork predicts carbon export with a  
829  $R^2$  of 0.69. **b,** The prokaryotic subnetwork predicts carbon export with a  $R^2$  of 0.60. **c,** The viral  
830 population subnetwork predicts carbon export with a  $R^2$  of 0.89.  
831

832 **Extended Data Figure 4:** *Synechococcus* (rather than *Prochlorococcus*) absolute cell counts  
833 correlate well to carbon export. **a,** *Prochlorococcus* cell counts estimated by flow cytometry do not  
834 correlate to carbon export (mean carbon flux at 150m, Pearson cor. = -0.13,  $p = 0.27$ ). **b,**  
835 *Synechococcus* cell counts estimated by flow cytometry correlate significantly to carbon export

836 (Pearson cor. = 0.64,  $p = 4.0 \times 10^{-10}$ ). **c**, *Synechococcus* / *Prochlorococcus* cell counts ratio correlates  
837 significantly to carbon export (Pearson cor. = 0.54,  $p = 4.0 \times 10^{-07}$ ).  
838

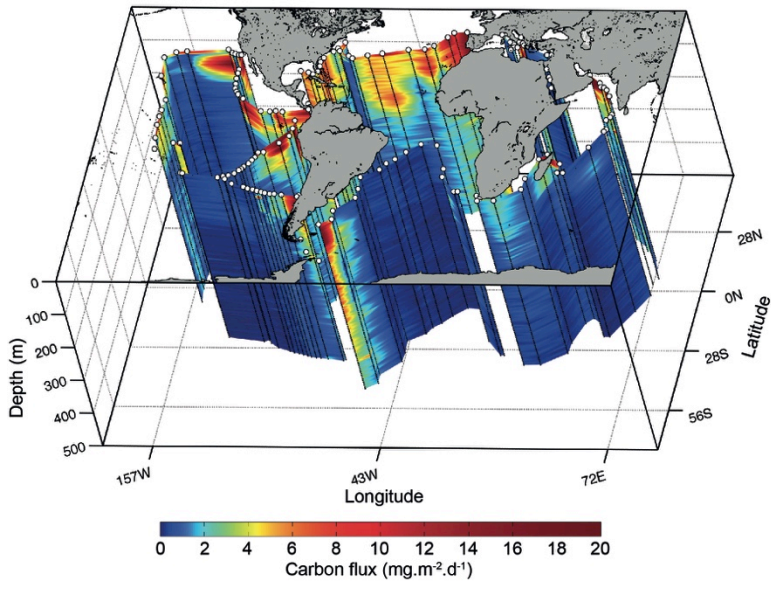
839 **Extended Data Figure 5:** Function and gene subnetworks associated to environmental parameters  
840 and their structure correlate to carbon export. **a,b**, Global ecological networks were built for the  
841 prokaryotic functions and viral PCs using the WGCNA methodology (see methods) and correlated to  
842 classical oceanographic parameters as well as carbon export. Each global network is decomposed into  
843 smaller coherent subnetworks (depicted by distinct colours on the y-axis) and their eigen vector is  
844 correlated to all environmental parameters. Similar to a correlation at the network scale, this approach  
845 directly links subnetworks to environmental parameters (*i.e.* the more the taxa contribute to the  
846 subnetwork structure, the more their abundance are correlated to the parameter). The measure allows  
847 to identify subnetworks for which the overall structure is related to the carbon export. **a**, Two  
848 bacterial functional subnetworks ( $n=441$  and  $n=220$ ,  $N=37'832$ ) are associated to carbon export  
849 (Pearson cor. 0.54,  $p = 1 \times 10^{-07}$  and 0.42,  $p = 1 \times 10^{-04}$ ). **b**, Two viral PCs subnetworks ( $n=1'879$  and  
850  $n=2'147$ ,  $N=4'678$ ) are strongly associated to carbon export (Pearson cor. 0.75,  $p = 3 \times 10^{-07}$  and 0.91,  $p =$   
851  $3 \times 10^{-14}$ ). **c,d** The WGCNA approach directly links subnetworks to environmental parameters, *i.e.* the  
852 more the features contribute to the subnetwork structure (topology), the more their abundance are  
853 correlated to the parameter. This measure allows to identify subnetworks for which the overall  
854 structure, summarized as the eigen vector of the subnetwork, is related to the carbon export. **c**, The  
855 bacterial function subnetwork structures correlates to carbon export (FNET1 Pearson cor. = 0.68,  $p =$   
856  $3 \times 10^{-61}$ , and FNET2 Pearson cor. = 0.47,  $p = 6 \times 10^{-13}$ ). **d**, The viral PC subnetwork structures correlates to  
857 carbon export (VNET1 Pearson cor. = 0.91,  $p < 1 \times 10^{-200}$ , and VNET2 Pearson cor. = 0.96,  $p < 1 \times 10^{-200}$ ).  
858

859 **Extended Data Figure 6:** Cumulative abundance of genus-level taxonomic annotations of genes  
860 encoding functions from FNET1 and FNET2 subnetworks and Bacterial function subnetworks  
861 predict carbon export. **a**, Genes contributing to the relative abundance of FNET1 and FNET2  
862 subnetwork functions were taxonomically annotated by homology searches against a non-redundant  
863 gene reference database using a last common ancestor (LCA) approach (see methods). **b,c**, PLS  
864 regression was used to predict carbon export using abundances of functions (OGs) in selected  
865 subnetworks. LOOCV was performed and VIP scores computed for each function. **b**, Light green  
866 subnetwork (FNET1) functions predict carbon export with a  $R^2$  of 0.41. **c**, Dark green subnetwork  
867 (FNET2) functions predict carbon export with a  $R^2$  of 0.48.  
868

869 **Extended Data Figure 7:** Viral protein cluster networks reveal potential marker genes for carbon  
870 export prediction at global scale. **a**, A viral protein cluster (PC) network was built using abundances  
871 of PCs predicted from viral population contigs associated to carbon export (Fig. 3b) using the  
872 WGCNA methodology (see methods) and correlated to classical oceanographic parameters. Two  
873 viral PC subnetworks (light and dark orange, VNET1 and VNET2, left and right panel respectively)  
874 are strongly associated to carbon export (VNET1: Pearson cor. 0.75,  $p = 3 \times 10^{-07}$  and VNET2: 0.91,  $p =$   
875  $3 \times 10^{-14}$ , Extended data figure 5b). Size of dots is proportional to the VIP score computed for the PLS  
876 regression. **b**, Viral PC subnetworks predict carbon export. PLS regression was used to predict  
877 carbon export using abundances of viral protein clusters (PCs) in selected subnetworks. LOOCV was  
878 performed and VIP scores computed for each PC. Light orange subnetwork (VNET1, left panel) PCs  
879 predict carbon export with a  $R^2$  of 0.55. Dark orange subnetwork (VNET2, right panel) PCs predict  
880 carbon export with a  $R^2$  of 0.89.  
881

882 **Extended Data Figure 8:** WGCNA and PLS regression analyses for the full Eukaryotic dataset. **a**, A  
883 single eukaryotic subnetwork ( $n=58$ , is strongly associated to carbon export (Pearson cor. 0.79,  $p =$   
884  $3 \times 10^{-14}$ ). **b**, The eukaryotic subnetwork structure correlates to carbon export (Pearson cor. = 0.94,  $p = 4 \times 10^{-27}$ ). **c**, The eukaryotic subnetwork predicts carbon export with a  $R^2$  of 0.76. **d**, Lineages with the  
885 highest VIP score (dots size is proportional to the VIP score in the scatter plot) in the PLS are  
886 depicted as red dots corresponding to two rhizarian (Collodaria), one copepod (*Euchaeta*), and three  
887 dinophyceae (*Noctiluca scintillans*, *Gonyaulax polygramma* and *Gonyaulax sp.* (clade 4)).  
888

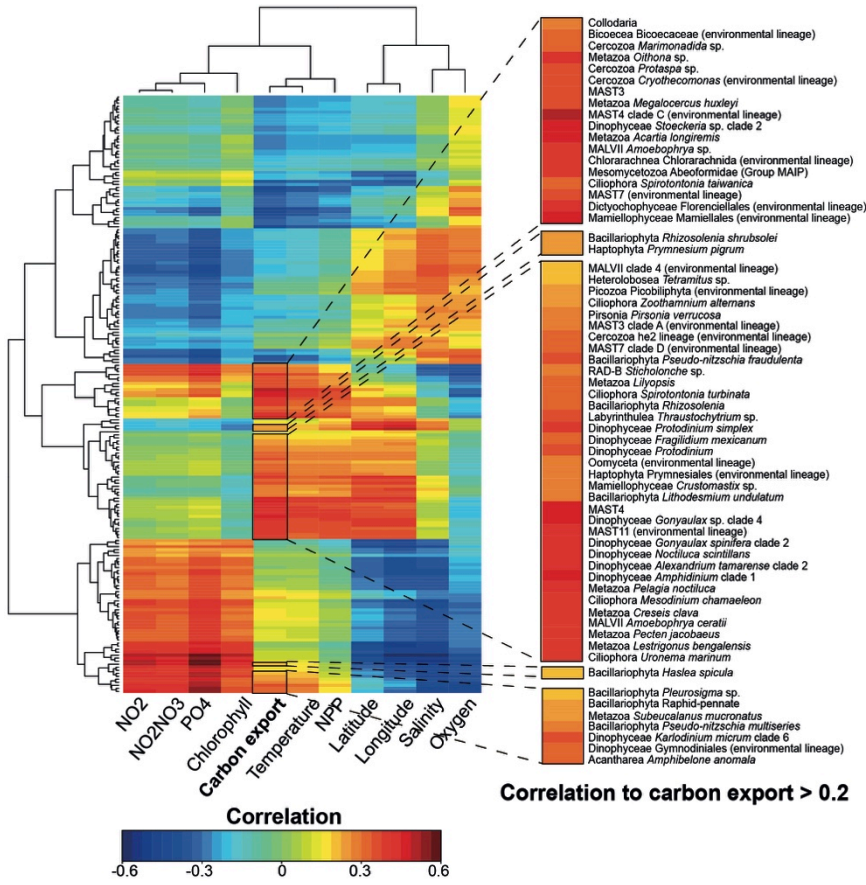
889



890

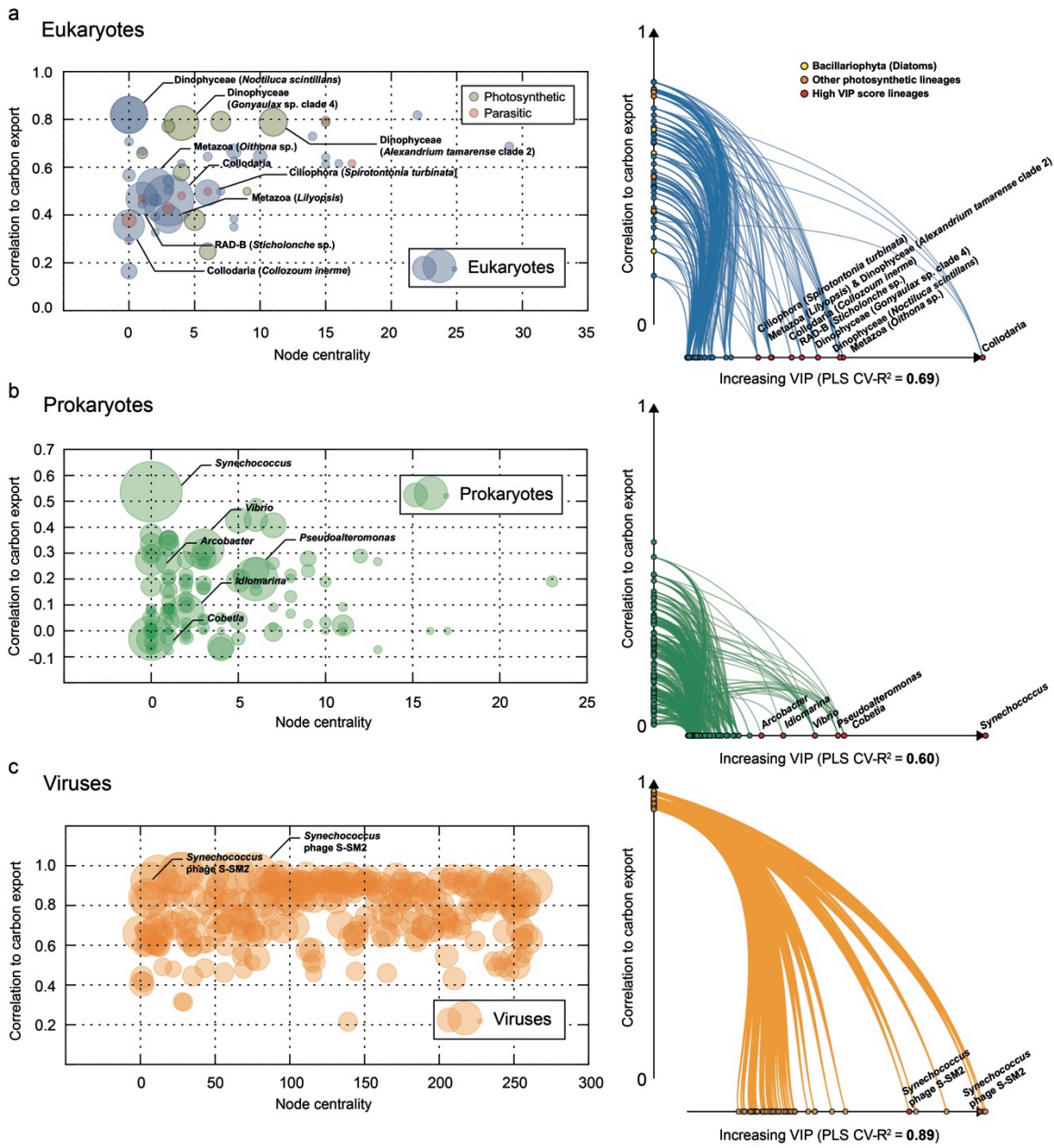
891 Figure 1

892



894  
895  
896  
897

Figure 2

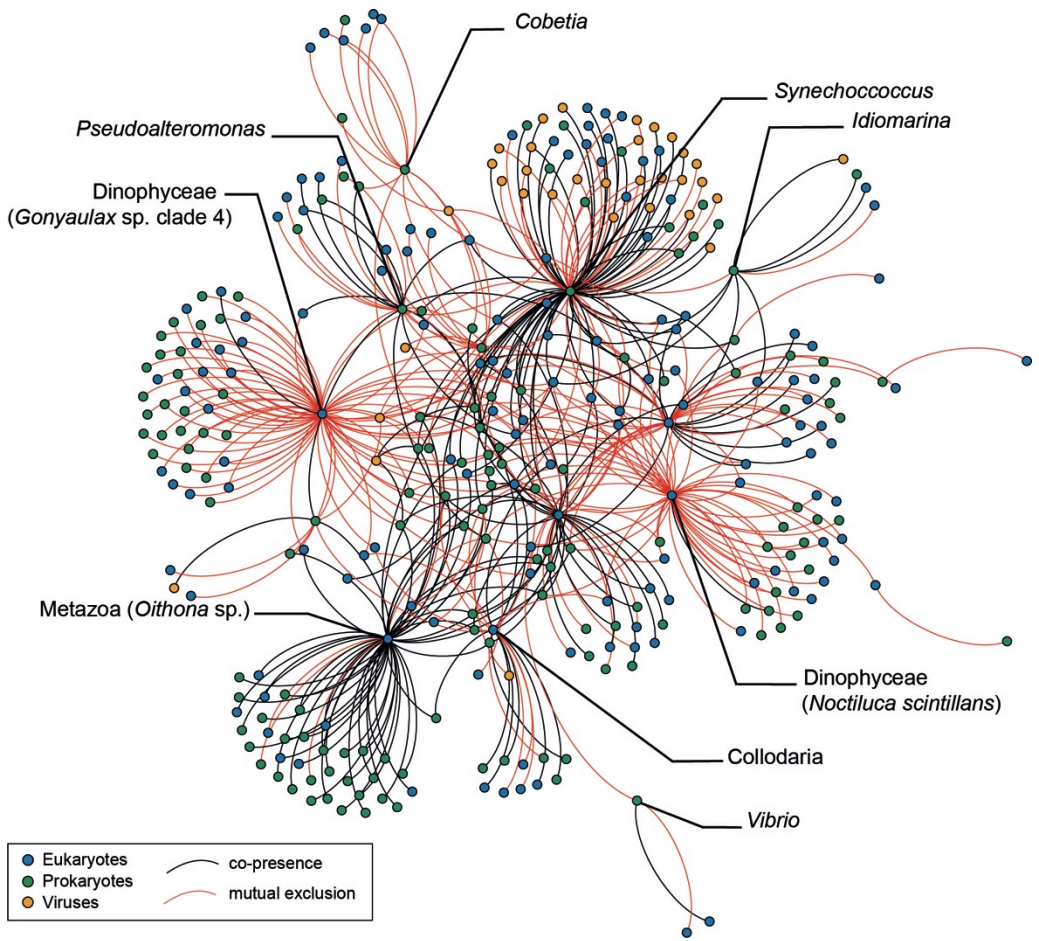


900

901 Figure 3

902

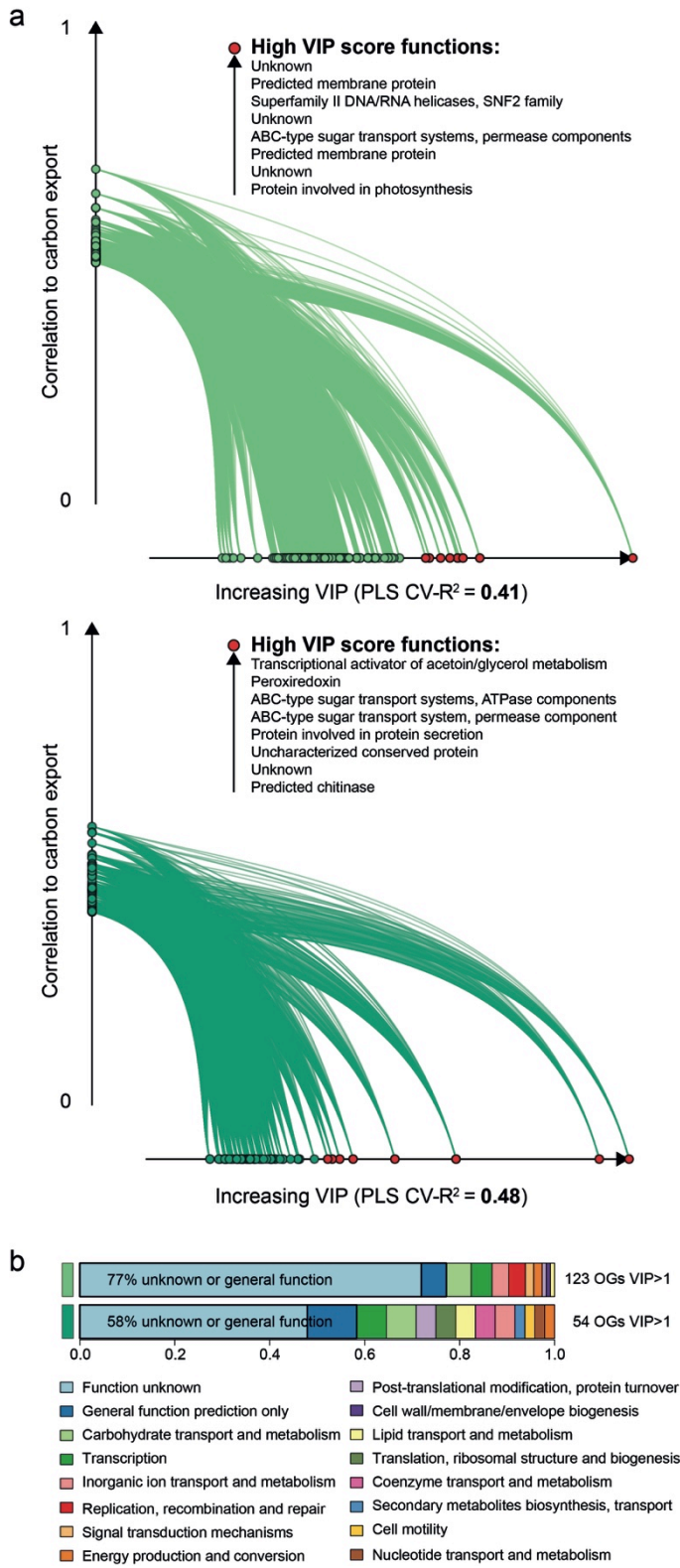
903  
904



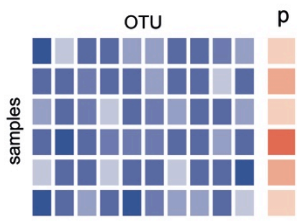
905

906 Figure 4

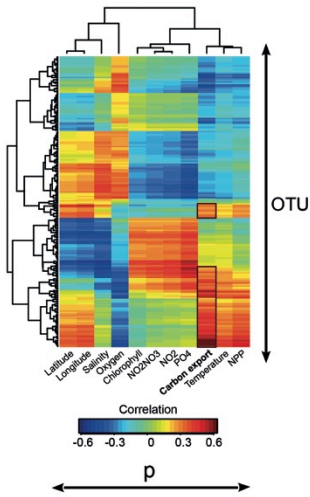
907



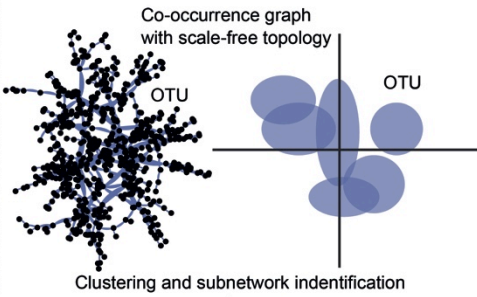
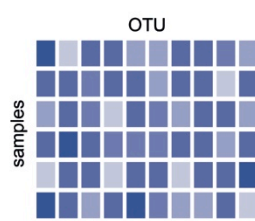
a) Pairwise approach



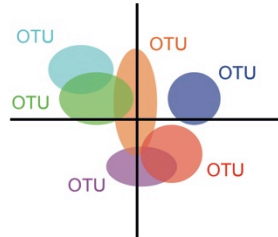
Correlation of OTU with environments



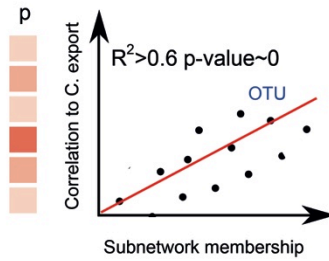
b) Graph-based approach (WGCNA)



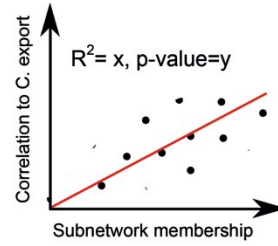
Clustering and subnetwork identification



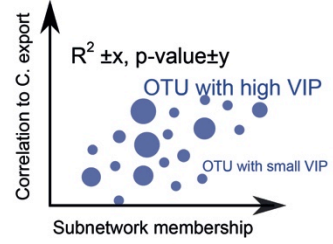
Relationship of the subnetwork topology and Carbon Export



c) Machine learning technique (PLS)



Reduction of OTU number while maintaining predictive power



913

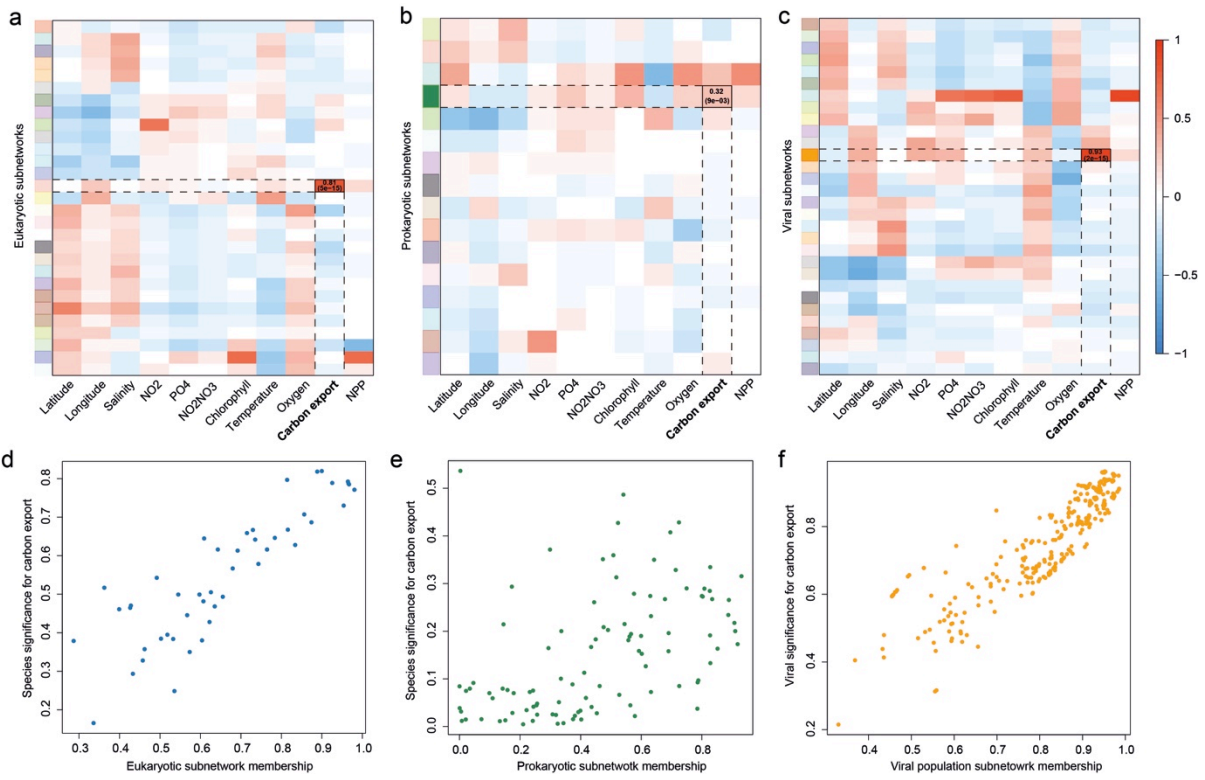
914 Extended Data Figure 1

915

916



917

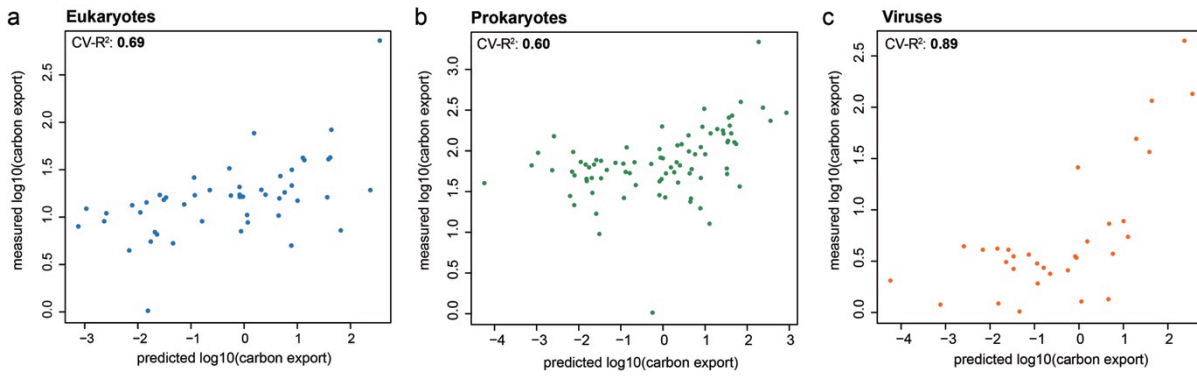


918

919 Extended Data Figure 2

920

921  
922

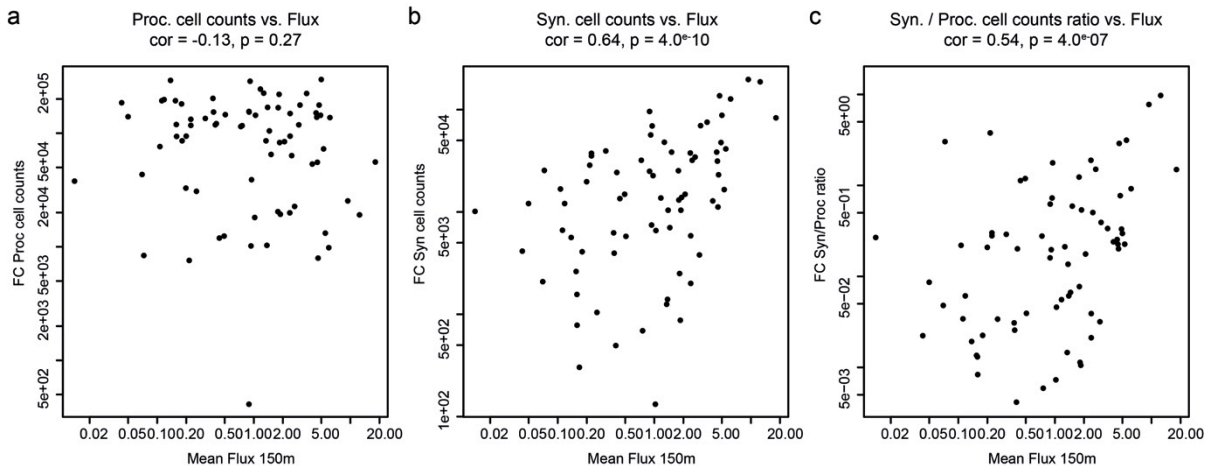


923

924 Extended Data Figure 3

925

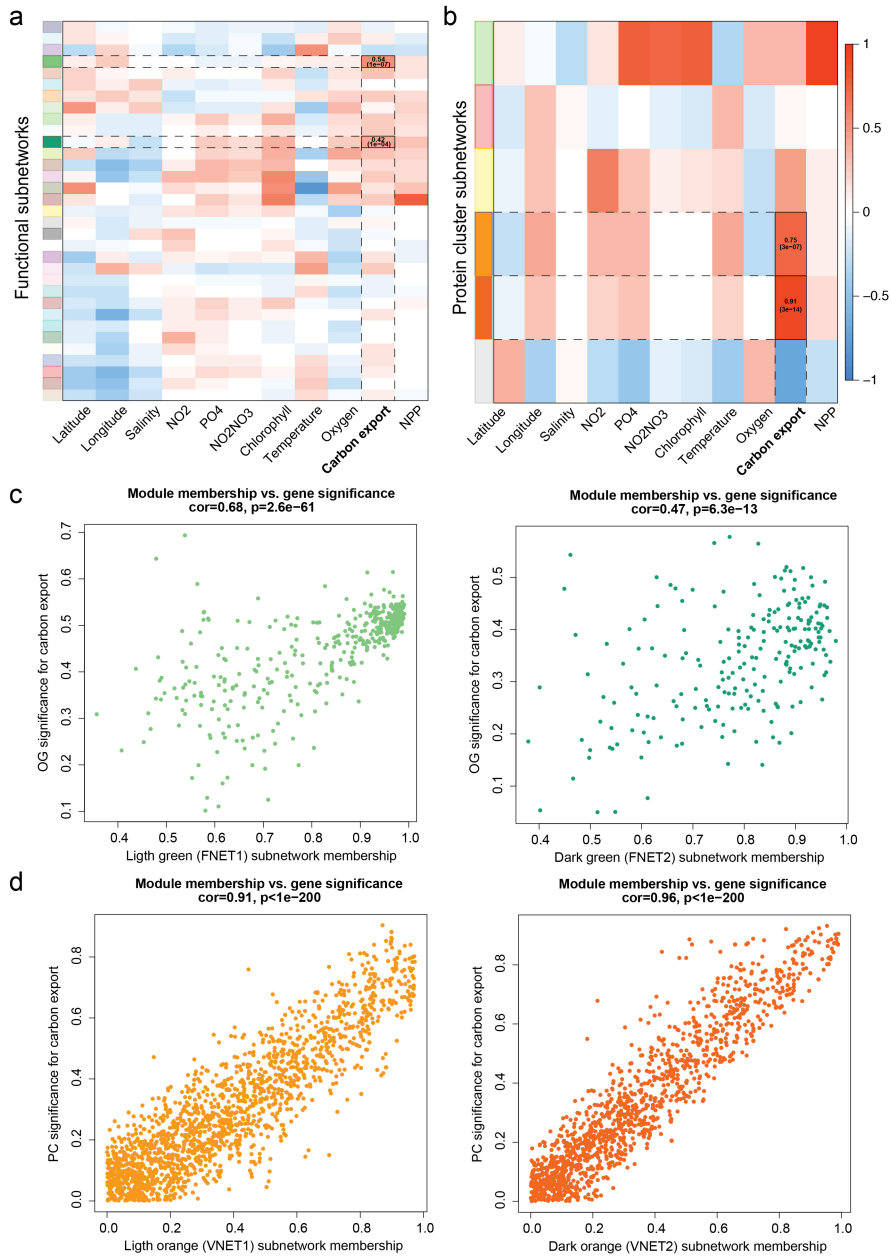
926  
927  
928



929

930 Extended Data Figure 4

931

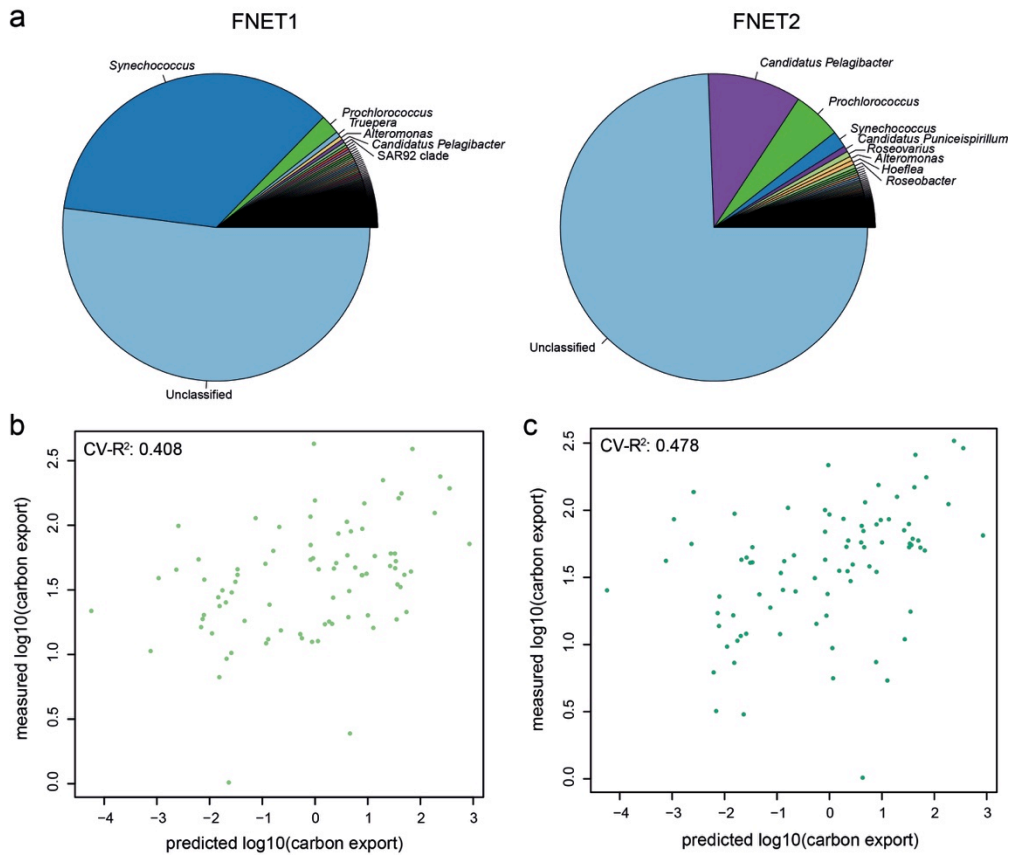


932

933 Extended Data Figure 5

934

935  
936

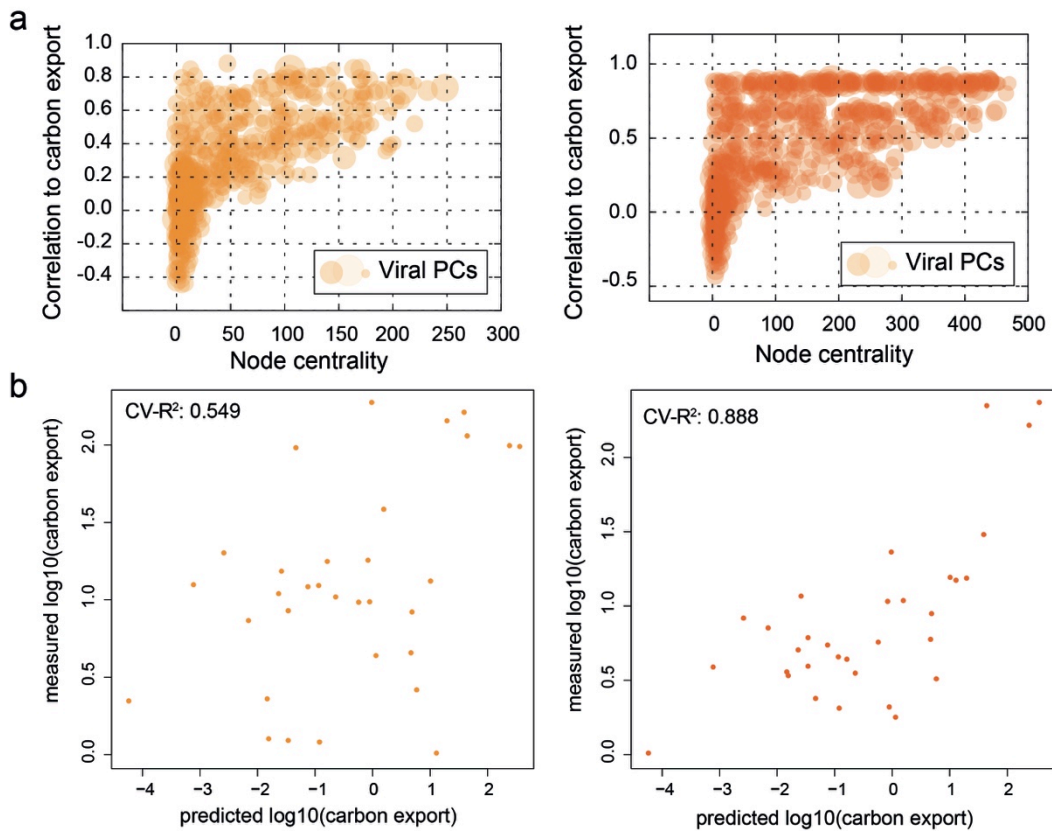


937

938 Extended Data Figure 6

939

940  
941

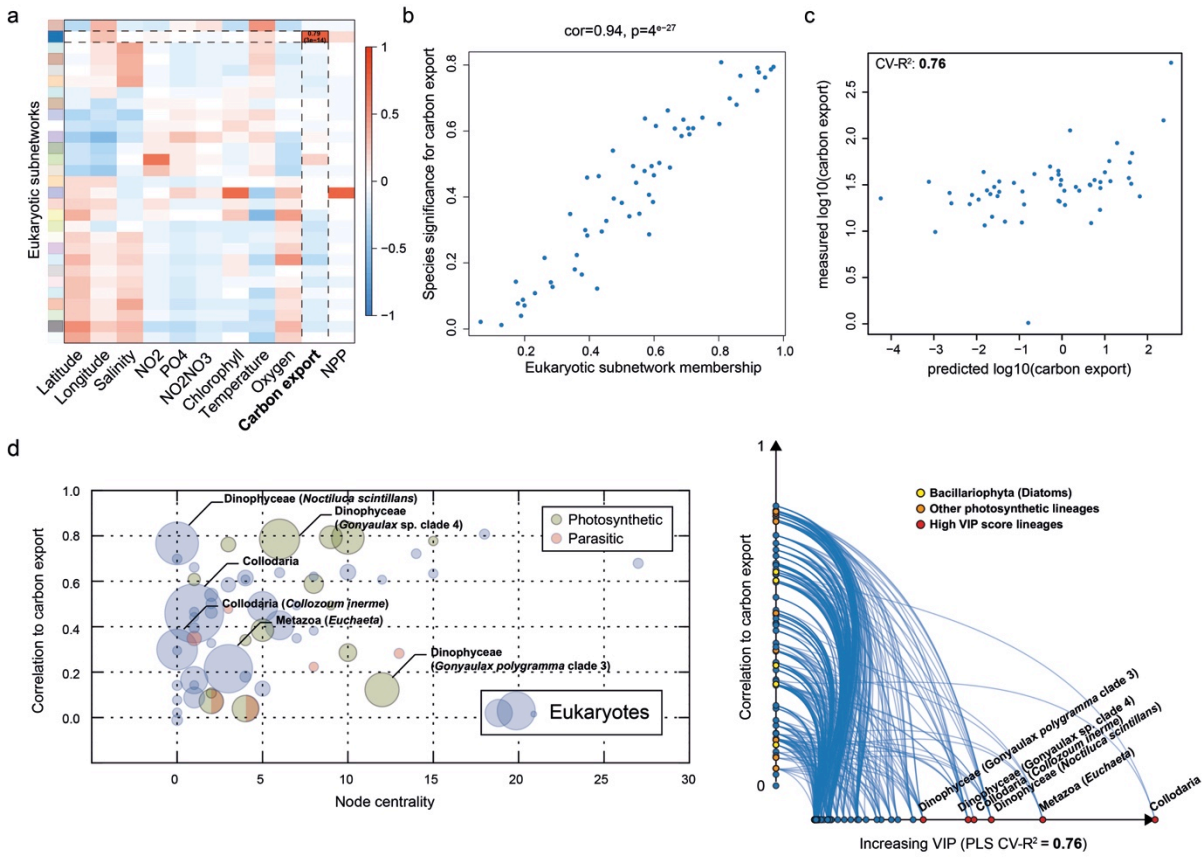


942

943 Extended Data Figure 7

944

945  
946



947

948 Extended Data Figure 8